AD-783 840

A HYSTERESIGRAPH FOR PLOTTING MAGNETIZATION CURVES

Reinhold W. Kubach

Dayton University

Prepared for:

Air Force Materials Laboratory

31 December 1966

DISTRIBUTED BY:

NTIS

National Technical Information Service
U. S. DEPARTMENT OF COMMERCE
5285 Port Royal Road, Springfield Va. 22151

NOTICE

When Government drawings, specifications, or other data are used for any purpose other than in connection with a definitely related Government procurement operation, the United States Government thereby incurs no responsibility nor any obligation whatsoever; and the fact that the Government may have formulated, furnished, or in any way supplied the said drawings, specifications, or other data, is not to be regarded by implication or otherwise as in any manner licensing the holder or any other person or corporation, or conveying any rights or permission to manufacture, use, or sell any patented invention that may in any way be related thereto.

ACCESSION for
NTIS White Section
DDC Buff Section
UNANNOUNCED
JUSTIFICATION .....
BY .....
DISTRIBUTION/AVAILABILITY CODES
Dist. AVAIL. and/or SPECIAL
A

Copies of this report should not be returned unless return is required by security considerations, contractual obligations, or notice on a specific document.

UNCLASSIFIED
Security Classification

AD 783840

DOCUMENT CONTROL DATA - R&D

(Security classification of title, body of abstract and indexing annotation must be entered when the overall report is classified)

1. ORIGINATING ACTIVITY *(Corporate author)*
University of Dayton Research Institute
300 College Park
Dayton, Ohio 45409

2a. REPORT SECURITY CLASSIFICATION
UNCLASSIFIED

2b. GROUP

3. REPORT TITLE
A HYSTERESIGRAPH FOR PLOTTING MAGNETIZATION CURVES

4. DESCRIPTIVE NOTES *(Type of report and inclusive dates)*
Technical Report 1 July 1966 to 31 December 1966

5. AUTHOR(S) *(Last name, first name, initial)*
KUBACH, REINHOLD W.

6. REPORT DATE
December 31, 1966

7a. TOTAL NO. OF PAGES
51

7b. NO. OF REFS
13

8a. CONTRACT OR GRANT NO.
AF 33(615)-~~5793~~ 3793

b. PROJECT NO.
7367

c.

d. 736703

9a. ORIGINATOR'S REPORT NUMBER(S)

9b. OTHER REPORT NO(S) *(Any other numbers that may be assigned this report)*

10. AVAILABILITY/LIMITATION NOTICES
This document has been approved for public release and sale; its distribution is unlimited.

11. SUPPLEMENTARY NOTES

12. SPONSORING MILITARY ACTIVITY
Air Force Materials Laboratory
Research and Technology Division
~~Air Force Systems Command~~
Wright-Patterson AFB, Ohio 45433

13. ABSTRACT

The objective of this study is to design, build, and calibrate a hysteresigraph for plotting magnetization curves of small cylindrical rod samples of dilute fine particle magnets. The magnetization of the sample and the field near its surface are measured with a set of balanced sensing coils. The voltages induced in these coils when the magnetic field is slowly changed are amplified and integrated electronically by means of two operational amplifiers (Miller integration), whose outputs drive an X-Y recorder.

The instrument must record hysteresis loops at peak field strengths up to 20,000 Oe with the expected values of coercive forces ranging from 100 to 10,000 Oe. The peak induction values may be expected to be in the range from 300 to 22,000 Gauss.

The instrument has been used to measure hysteresis loops of various permanent magnets, and coercive forces of powdered rare earth-cobalt alloys which are under development as new magnetic materials.

Reproduced by
NATIONAL TECHNICAL
INFORMATION SERVICE
U S Department of Commerce
Springfield VA 22151

DD FORM 1 JAN 64 1473

UNCLASSIFIED
Security Classification

UNCLASSIFIED

Security Classification

14. KEY WORDS	LINK A ROLE	LINK A WT	LINK B ROLE	LINK B WT	LINK C ROLE	LINK C WT
Hysteresigraph						
Ferromagnetic Materials						
Magnetization curves						

INSTRUCTIONS

1. ORIGINATING ACTIVITY: Enter the name and address of the contractor, subcontractor, grantee, Department of Defense activity or other organization *(corporate author)* issuing the report.

2a. REPORT SECURITY CLASSIFICATION: Enter the overall security classification of the report. Indicate whether "Restricted Data" is included. Marking is to be in accordance with appropriate security regulations.

2b. GROUP: Automatic downgrading is specified in DoD Directive 5200.10 and Armed Forces Industrial Manual. Enter the group number. Also, when applicable, show that optional markings have been used for Group 3 and Group 4 as authorized.

3. REPORT TITLE: Enter the complete report title in all capital letters. Titles in all cases should be unclassified. If a meaningful title cannot be selected without classification, show title classification in all capitals in parenthesis immediately following the title.

4. DESCRIPTIVE NOTES: If appropriate, enter the type of report, e.g., interim, progress, summary, annual, or final. Give the inclusive dates when a specific reporting period is covered.

5. AUTHOR(S): Enter the name(s) of author(s) as shown on or in the report. Enter last name, first name, middle initial. If military, show rank and branch of service. The name of the principal author is an absolute minimum requirement.

6. REPORT DATE: Enter the date of the report as day, month, year; or month, year. If more than one date appears on the report, use date of publication.

7a. TOTAL NUMBER OF PAGES: The total page count should follow normal pagination procedures, i.e., enter the number of pages containing information.

7b. NUMBER OF REFERENCES: Enter the total number of references cited in the report.

8a. CONTRACT OR GRANT NUMBER: If appropriate, enter the applicable number of the contract or grant under which the report was written.

8b, 8c, & 8d. PROJECT NUMBER: Enter the appropriate military department identification, such as project number, subproject number, system numbers, task number, etc.

9a. ORIGINATOR'S REPORT NUMBER(S): Enter the official report number by which the document will be identified and controlled by the originating activity. This number must be unique to this report.

9b. OTHER REPORT NUMBER(S): If the report has been assigned any other report numbers *(either by the originator or by the sponsor)*, also enter this number(s).

10. AVAILABILITY/LIMITATION NOTICES: Enter any limitations on further dissemination of the report, other than those imposed by security classification, using standard statements such as:

(1) "Qualified requesters may obtain copies of this report from DDC."

(2) "Foreign announcement and dissemination of this report by DDC is not authorized."

(3) "U. S. Government agencies may obtain copies of this report directly from DDC. Other qualified DDC users shall request through _____."

(4) "U. S. military agencies may obtain copies of this report directly from DDC. Other qualified users shall request through _____."

(5) "All distribution of this report is controlled. Qualified DDC users shall request through _____."

If the report has been furnished to the Office of Technical Services, Department of Commerce, for sale to the public, indicate this fact and enter the price, if known.

11. SUPPLEMENTARY NOTES: Use for additional explanatory notes.

12. SPONSORING MILITARY ACTIVITY: Enter the name of the departmental project office or laboratory sponsoring *(paying for)* the research and development. Include address.

13. ABSTRACT: Enter an abstract giving a brief and factual summary of the document indicative of the report, even though it may also appear elsewhere in the body of the technical report. If additional space is required, a continuation sheet shall be attached.

It is highly desirable that the abstract of classified reports be unclassified. Each paragraph of the abstract shall end with an indication of the military security classification of the information in the paragraph, represented as *(TS), (S), (C), or (U)*.

There is no limitation on the length of the abstract. However, the suggested length is from 150 to 225 words.

14. KEY WORDS: Key words are technically meaningful terms or short phrases that characterize a report and may be used as index entries for cataloging the report. Key words must be selected so that no security classification is required. Identifiers, such as equipment model designation, trade name, military project code name, geographic location, may be used as key words but will be followed by an indication of technical context. The assignment of links, rules, and weights is optional.

ia

UNCLASSIFIED

Security Classification

AFLC-WPAFB-OCT 66 6M

A HYSTERESIGRAPH FOR PLOTTING MAGNETIZATION CURVES

Reinhold W. Kubach
University of Dayton

This document has been approved for public release and sale; its distribution is unlimited.

ib

FOREWORD

The work described in this report was carried out in the laboratories of the Material Physics Division under USAF Contract No. AF 33(615)-3793 entitled "Research on Intermediate Phases of Rare Earth Metals". This contract was initiated under Project No. 7367, "Research on the Characterization and Properties of Materials", Task No. 736703, "Electronic and Magnetic Properties of Materials".

The work was administered by the Air Force Materials Laboratory, Research and Technology Division, Air Force Systems Command, Wright-Patterson Air Force Base, Ohio, Dr. Karl Strnat, Project Engineer.

This report covers work conducted during the period July 1, 1966 to December 31, 1966. The manuscript was released by the author in December 1966 for publication as a technical report.

The author is indebted to Dr. Karl Strnat of the Air Force Materials Laboratory for helpful discussions and to Mr. John C. Olson for his assistance in building the apparatus and preparation of the samples. Special thanks are due the management of the Electromagnetic Materials Branch for the use of its facilities.

This technical report has been reviewed and is approved.

David J. Iden

Major David J. Iden
Chief, Electromagnetic Materials Branch
Materials Physics Division
Air Force Materials Laboratory

ABSTRACT

The objective of this study is to design, build, and calibrate a hysteresigraph for plotting magnetization curves of small cylindrical rod samples of dilute fine particle magnets. The magnetization of the sample and the field near its surface are measured with a set of balanced sensing coils. The voltages induced in these coils when the magnetic field is slowly changed are amplified and integrated electronically by means of two operational amplifiers (Miller integration), whose outputs drive an X-Y recorder.

The instrument must record hysteresis loops at peak field strengths up to 20,000 Oe with the expected values of coercive forces ranging from 100 to 10,000 Oe. The peak induction values may be expected to be in the range from 300 to 22,000 Gauss.

The instrument has been used to measure hysteresis loops of various permanent magnets, and coercive forces of powdered rare earth-cobalt alloys which are under development as new magnetic materials.

TABLE OF CONTENTS

Title	Page
SECTION I INTRODUCTION	1.
1. HYSTERESIS LOOPS AND MAGNETIC MATERIALS	1.
2. SPECIFIC AIM OF PROJECT	1.
3. DESIGN SPECIFICATIONS	2.
SECTION II BASIC CONCEPTS OF MAGNETIC MEASUREMENTS	4.
SECTION III THEORY OF HYSTERESIGRAPH	8.
1. SCHEMATIC OF A HYSTERESIGRAPH	8.
2. SENSING COILS	8.
3. ELECTRONIC INTEGRATION	10.
4. ANALYSIS OF INTEGRATOR ERROR	17.
SECTION IV DESIGN AND CONSTRUCTION OF THE HYSTERESIGRAPH	19.
1. RECORDER AND AMPLIFIERS	19.
2. DETERMINATION OF INTEGRATING NETWORKS	19.
3. INTEGRATOR PERFORMANCE	21.
4. COIL CONSTRUCTION	23.
5. COIL COMPENSATION	26.
SECTION V CALIBRATION OF THE HYSTERESIGRAPH	31.
1. CALIBRATING PROCEDURE	31.
2. CALIBRATING THE H COIL	31.
3. CALIBRATING THE (B-H) COIL	31.

TABLE OF CONTENTS (con't)

Title	Page
4. OVERALL ACCURACY	33.
SECTION VI OPERATION OF THE HYSTERESIGRAPH	34.
SECTION VII SUMMARY	38.
1. SIGNIFICANCE OF THIS CONTRIBUTION	38.
2. RECOMMENDATIONS FOR FURTHER STUDY	38.
3. FUTURE USE	39.
BIBLIOGRAPHY	40.

LIST OF FIGURES

Figure		Page
1.	Typical Hysteresis Loops (a) B Versus H Loop (b) $4\pi M$ Versus H Loop	2.
2.	Basic Circuit for Measuring B Versus H Loops of Ring Shaped Samples	5.
3.	Simplified Schematic of Hysteresigraph for the Measurement of B Versus H Loops	5.
4.	Schematic Arrangement for Measuring Surface B and H Fields of Rod Samples	6.
5.	Elementary Hysteresigraph for Plotting B Versus H Loops of Rod Samples	7.
6.	Elementary Hysteresigraph for Plotting $4\pi M$ Versus H Loops	8.
7.	Arrangement of Sensing Coils for Measuring Surface B and H Fields of Rod Samples	9.
8.	General Operational Amplifier	11.
9.	Approximate Equivalent Circuit of Operational Amplifier	13.
10.	Approximate Equivalent Circuit of Integrating Operational Amplifier	14.
11.	Integrating Operational Amplifier Circuit	14.
12.	Equivalent Circuit of General Operational Amplifier	15.
13.	Equivalent Circuit of Miller Integrator	16.
14.	Passive Integrating Circuit	16.
15.	Integration of a Step Function	17.
16.	Response of Miller Integrator to Step Input (Long Time Integration)	22.

LIST OF FIGURES (con't)

Figure		Page
17.	Response of Miller Integrator to Step Input (Short Time Integration)	24.
18.	(a) Cross Section of Coil Arrangement (b) Coil Form	25.
19.	Remaining Coil Imbalance	27.
20.	Schematic of Hysteresigraph	29.
21.	Magnet and Hysteresigraph Set Up for Testing	30.
22.	Coil Calibration Curves	32.
23.	$4\pi M$ Versus H Loop of a Typical Ce (Ce-Rich Mischmetal) Co_5 Sample	35.
24.	$4\pi M$ Versus H Loop of a Typical Alnico VI Sample	36.
25.	$4\pi M$ Versus H Loop of a Typical $SmCo_5$ Sample	37.

SECTION I

INTRODUCTION

1. HYSTERESIS LOOPS AND MAGNETIC MATERIALS

Hysteresis loops provide essential information which quantitatively describe the properties of ferromagnetic materials as indicated in Figure 1. Consequently the measurement of hysteresis loops constitutes one of the major tasks in the development of magnetic materials. Reference to Figure 1 also shows that there are two ways of plotting hysteresis loops. In one version, loop (a), the magnetic induction B (measured in Gauss) is plotted as a function of the exciting field H (measured in Oersted). In this form the hysteresis loop is most useful to the engineer engaged in the design of magnetic circuits. In the other version, loop (b), the intrinsic induction, $4\pi M$ (in Gauss) is plotted versus the field H (in Oersted). M, the magnetization or the magnetic moment per unit volume is measured in $\frac{emu}{cm^3} = 4\pi$ Gauss and is related to the induction B by the equation

$$B = H + 4\pi M \tag{1}$$

Since the magnetization M and the coercive force ${}_MH_c$ are closely related to the microscopic properties of the material, $4\pi M$ versus H plots are most important to the physicist engaged in research and development of magnetic materials.

The data for plotting hysteresis loops were previously obtained by a point-by-point measurement method which was tedious and time-consuming. For this reason instruments known as hysteresigraphs for drawing B versus H loops automatically were developed.

2. SPECIFIC AIM OF PROJECT

The hysteresigraph to be described here was exclusively developed for plotting $4\pi M$ versus H loops. None of the hysteresigraphs reported in the literature were readily adaptable for this use, nor were they commercially available. Furthermore, the particular application of this instrument created additional design problems which are not characteristic of those reported in the literature (References 1 - 4). This new type of hysteresigraph is used in an extensive research program conducted at the Air Force Materials Laboratory, aimed at finding new materials for possible use as permanent magnets (Reference 5). One phase of this program deals with the systematic evaluation of the magnetic properties of crystal anisotropy-controlled powder magnets of the rare earth-cobalt intermetallic compounds YCo_5, $SmCo_5$, Ce (Ce-rich mischmetal) Co_5 and others. A large number of samples are to be

tested which are typically 15mm long x 11mm diameter, and only a small packing fraction (typically 5 v/o) is active magnetic material.

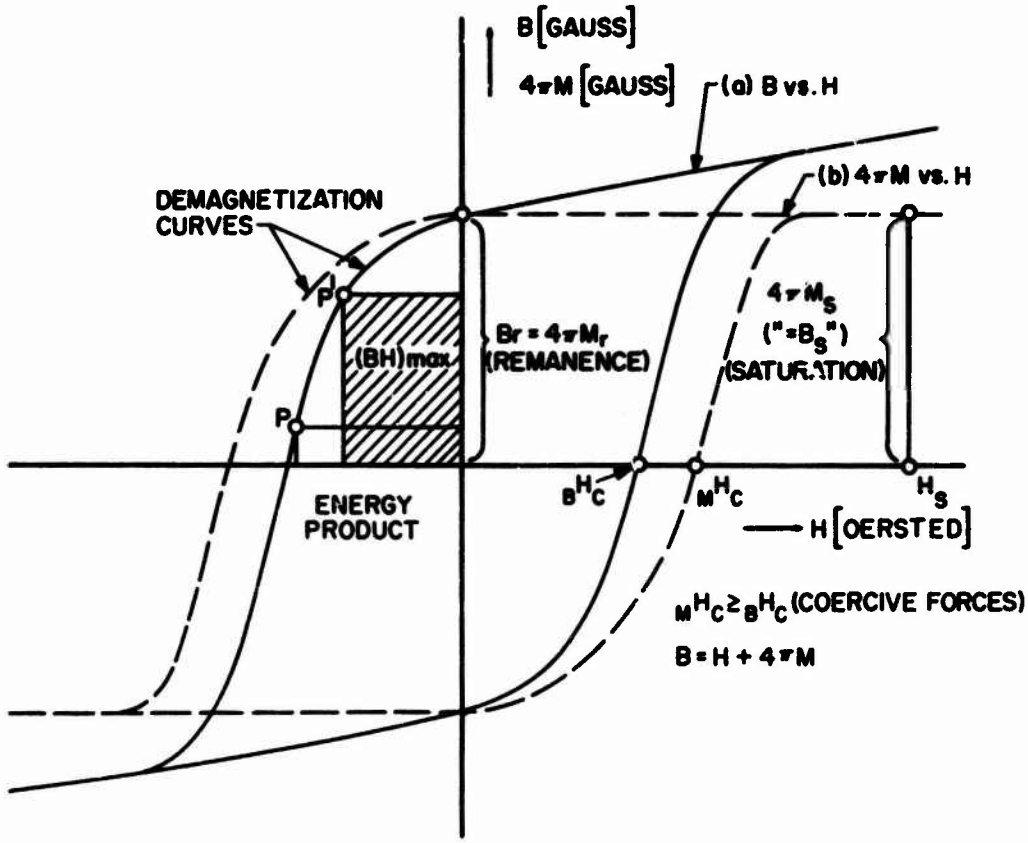

Figure 1. Typical Hysteresis Loops (a) B Versus H Loop
(b) 4πM Versus H Loop

Thus the new hysteresigraph has to be capable of plotting 4πM versus H loops of extremely "weak" magnets, but also dense and "strong" magnets.

3. DESIGN SPECIFICATIONS

Because of the wide scope of the entire program the specifications for this instrument were rather severe. The design specifications were as follows:

a) Obtain 4πM versus H loops of dilute, i.e., weak magnets which permit one to measure coercive forces ${}_MH_c$ over the range of 100-10,000 Oe at $H_m \approx 30,000$ Oe. The expected range of $4\pi M_s = B_s = 6000 - 21,500$ Gauss for the magnetic portion of the sample which is present at packing fractions of ≈5%. The values of ${}_MH_c$ should be readable to ± 5 Oe. Measurement of the small 4πM signals may be highly inaccurate (± 25%).

b) Obtain $4\pi M$ versus H loops for dense magnets, having packing fractions of 30-100%, with high accuracy for the H-measurement ($\pm$ 5 Oe) as well as the $4\pi M$-measurement ($\pm$ 20 G). From these curves B versus H loops are to be derived and the energy product determined.

SECTION II

BASIC CONCEPTS OF MAGNETIC MEASUREMENTS

The quantities B and H are conveniently found by measuring the induced voltage in a coil. The instantaneous voltage, e, induced in a coil of N turns, when the magnetic flux ϕ is changing, is given by Faraday's law as

$$e = -N\frac{d\phi}{dt} \cdot \times 10^{-8} \quad \text{volts} \tag{2}$$

Faraday's law holds whether the coil is stationary and the flux changes or the coil is moved through a uniform but time invariant field. The flux change is found by integrating Equation (2) as

$$d\phi = -\frac{10^8}{N}\int_{t_1}^{t_2} e\,dt \tag{3}$$

which can be written as

$$\Delta\phi = \phi_1 - \phi_2 = \frac{10^8}{N}\int_{t_1}^{t_2} e\,dt \tag{4}$$

The change in flux density B is obtained from Equation (4) as

$$\Delta B = \frac{\Delta\phi}{A} = \frac{10^8}{NA}\int_{t_1}^{t_2} e\,dt \tag{5}$$

where A is the cross-sectional area of the test sample in cm^2. It follows from Equation (5) that ΔB is determined if $\int e\,dt$ can be measured.

The classical instrument for performing the integration $\int e\,dt$ is the ballistic galvanometer. Commercial flux meters differ from the basic ballistic galvanometer on account of their much heavier electrical damping, the torque compensation of their moving coil suspension, and their portability.

B versus H loops can be measured with such a flux meter when it is used in a circuit as shown in Figure 2. In this arrangement the ring-shaped test sample of magnetic material carries two windings. The primary winding (P) is connected to an adjustable constant current supply and the secondary winding (S) is connected to a flux meter. The field strength H is calculated from the relation

$$H = \frac{4\pi Ni}{10 \times L} \tag{6}$$

where N is the number of turns on the primary winding, 'i' is the current as measured by the ammeter A, and L is the mean magnetic path length. When H is suddenly changed from one value to another, the resulting change in B induces a voltage in the secondary winding which according

to Equation (5) is proportional to the change in B. For a detailed description of the methods which are commonly used to establish enough points from which a B versus H loop can be drawn, the reader is referred to Reference 6. The disadvantages, some of which have been pointed out in Section I, have led to the development of hysteresigraphs for plotting B versus H loops.

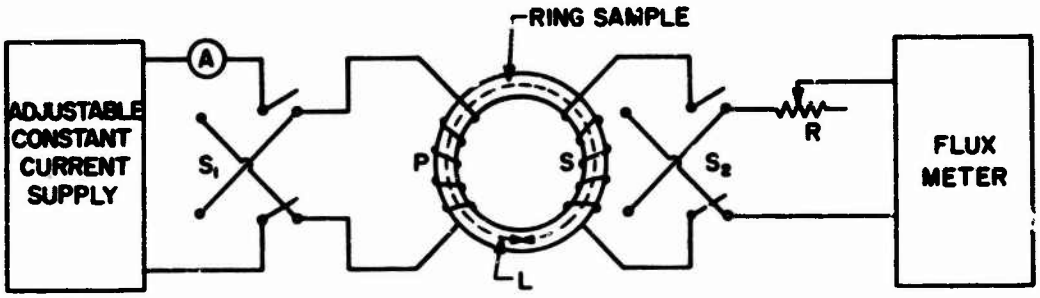

Figure 2. Basic Circuit for Measuring B Versus H Loops of Ring Shaped Samples

Most of the hysteresigraphs for the measurement of B versus H loops are built around the basic diagram shown in Figure 3. From an inspection of this diagram it is seen that the field intensity H is measured in terms of the voltage e_H which is developed by the exciting current and applied to the X-axis of the recorder. The induction B is measured by applying the induced voltage e_B to the integrator and $\int e_B dt$ to the Y-axis of the recorder.

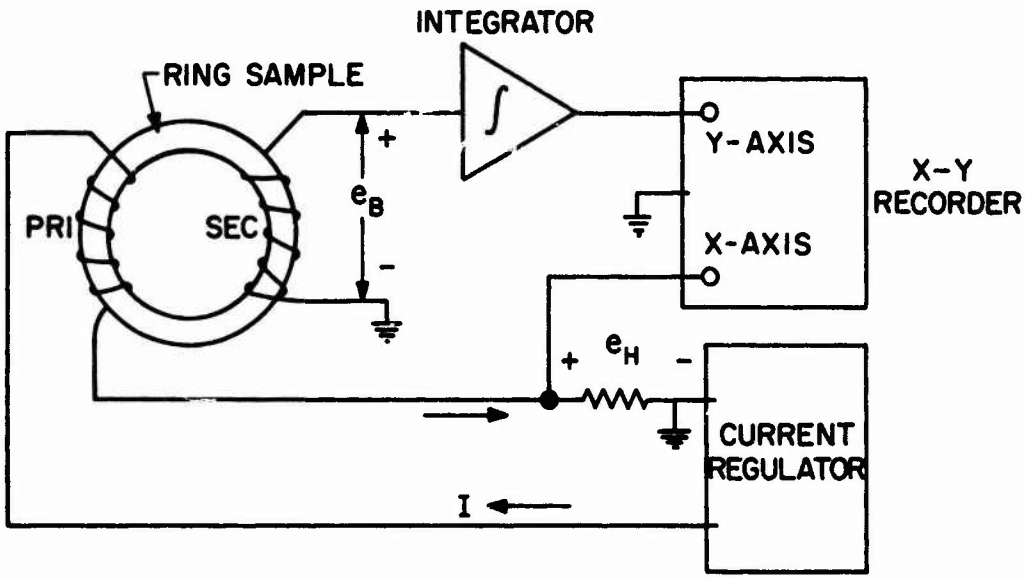

Figure 3. Simplified Schematic of Hysteresigraph for the Measurement of B Versus H Loops

This system as it stands is not suitable for rapid testing of large numbers of test specimens, because of the time required to machine

and wind each ring. Furthermore, large field intensities as are required for testing permanent magnets cannot be produced by the primary winding, as the necessary number of turns or the required current become prohibitively large. Consequently hard magnetic materials are being tested in strong and homogeneous fields of the order of 10-20 kOe which can easily be produced between the pole caps of electromagnets, thus necessitating cylindrical rod samples rather than ring samples. Under these circumstances the measurement of the field intensity H becomes more difficult because the H field between the pole caps will be disturbed by the sample's own stray field, known as the demagnetizing field. The H field referred to in Equation (1) is the true internal field H_i of the sample and not the applied field H_a. These two fields differ from each other by the sample's demagnetizing field H_d according to the relation

$$H_i = H_a - H_d \tag{7}$$

The demagnetizing field is given by

$$H_d = DM \tag{8}$$

where D is the demagnetizing factor and M is the magnetization of the sample. The demagnetizing factor is well defined for ellipsoids; for other sample geometries in which M is not uniform throughout, the demagnetizing factor is not an exact concept. In practice, average values of D are ascribed to the various geometries in order to indicate the magnitude of the internal field (Reference 7).

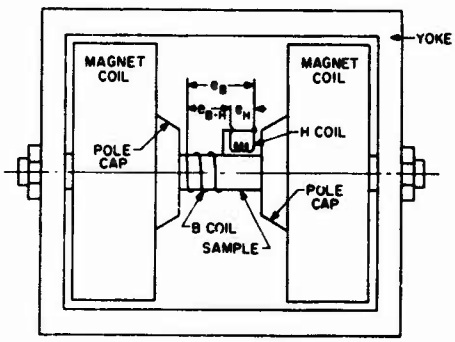

Figure 4. Schematic Arrangement for Measuring Surface B and H Fields of Rod Samples

If M is to characterize the material properties independently of sample shape or size, $4\pi M$ must be plotted as a function of H_i and not H_a. It is thus necessary either to correct mathematically for the demagnetizing factor or to try to measure H_i directly. The first method can be applied to ellipsoidal samples but becomes questionable for cylindrical rods. Thus, for cylindrical rods, H_i should be measured directly. Since it is impossible to measure H_i by placing a probe

within the sample, another alternative makes use of the fact that the tangential component of the H field goes unchanged through the interface of two substances. This follows from Maxwell's equations in the electromagnetic field theory (Reference 7). Thus in the center of the rod length where the total H is tangent to the surface, the field in the air just outside the sample is identical with the H field in the material. A schematic for measuring the surface B and H fields of rod samples in an electromagnet is shown in Figure 4.

Utilization of a coil arrangement consisting of a B coil and an annular H coil to be described later in Section III, makes it possible to measure these fields quite accurately in terms of the induced voltages e_B and e_H respectively. If each of these induced voltages is applied to its own integrator and recorder channel, the result is a hysteresigraph for plotting B versus H loops of rod samples as shown in Figure 5.

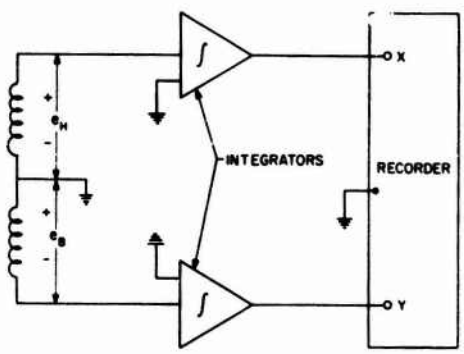

Figure 5. Elementary Hysteresigraph for Plotting B Versus H Loops of Rod Samples

To plot $4\pi M$ versus H loops of rod samples requires that the annular H coil and the B coil be interconnected and matched to measure $4\pi M = B - H$.

SECTION III

THEORY OF HYSTERESIGRAPH

1. SCHEMATIC OF A HYSTERESIGRAPH

From the development of the previous section a tentative schematic of a hysteresigraph for plotting $4\pi M$ versus H loops can be drawn as shown in Figure 6. Whereas the system of Figure 6 is in principle straightforward, its realization is not, because of problems arising from the measurement of $4\pi M$ and problems arising from the application of this system to weak permanent magnets.

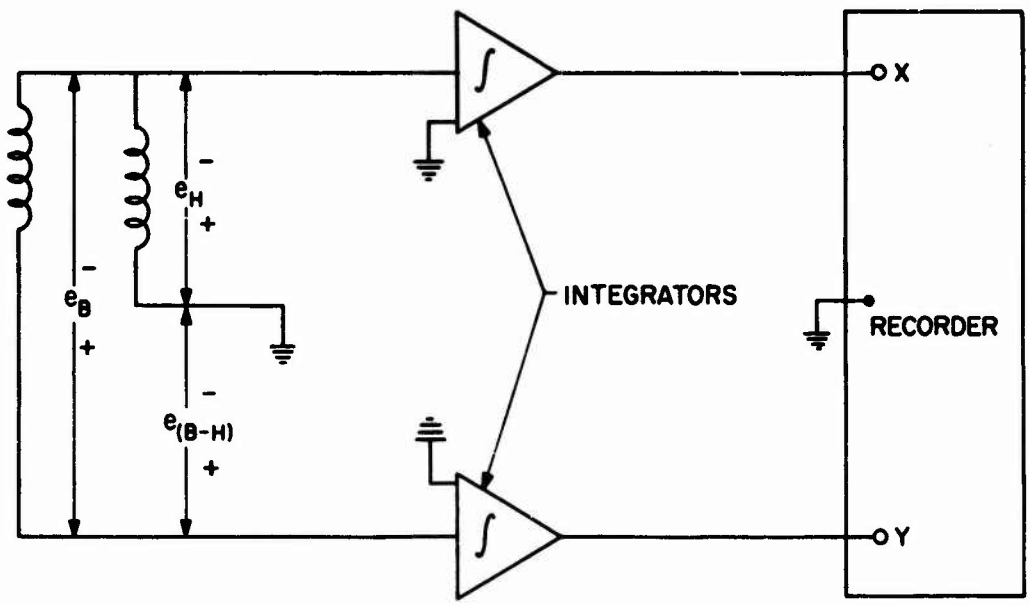

Figure 6. Elementary Hysteresigraph for Plotting $4\pi M$ Versus H Loops

Since $4\pi M$ cannot be measured directly, its determination hinges on the ability to measure the "true" B and H fields on the surface of the sample. The design and calibration of a coil arrangement capable of producing voltages proportional to H, B and B-H contributes the most important, and as it turns out, the most difficult part of the entire hysteresigraph construction.

2. SENSING COILS

The coil arrangement of the hysteresigraph shown in Figure 6 consists of two coils referred to as the annular H coil and the B coil and used for the measurement of the B and H fields on the surface of the sample. If these two coils are interconnected in series opposition,

a voltage proportional to $4\pi M$ is obtained according to the relation

$$4\pi M = B - H \tag{9}$$

H is here the internal field H_i, which is reasonably well represented by the field near the surface of the sample as measured by our coil. B is the magnetic induction of the sample induced by the H field. The annular H coil if formed from two individual windings, having identical numbers of turns N_H, referred to as outer H winding (Ho) and inner H winding (Hi) respectively, as shown in Figure 7. If these two coils are connected in series opposition, the voltage induced in them is given by

$$e_H = e_{Ho} - e_{Hi} = - \frac{d}{dt} (\lambda Ho - \lambda Hi) \tag{10}$$

where $\frac{d}{dt}(\lambda Ho)$ and $\frac{d}{dt}(\lambda Hi)$ are the time rate of change of the flux linkages of the Ho and Hi windings respectively. Since in general $\lambda = N\phi = NBA$ and for a uniform field in air B=H, Equation (10) can be written as

$$e_H = - \frac{d}{dt} H(Ao - Ai)N_H \tag{11}$$

where Ao and Ai are the cross-sectional areas of the Ho and Hi windings respectively, and N_H are the number of turns each of the Ho and Hi windings. It is seen from Equation (11) that the terminal voltage of the annular H coil in Figure 7 is proportional to the change in flux linkages through the annulus formed by the two windings, and can therefore be used to measure the H field at the surface of the sample.

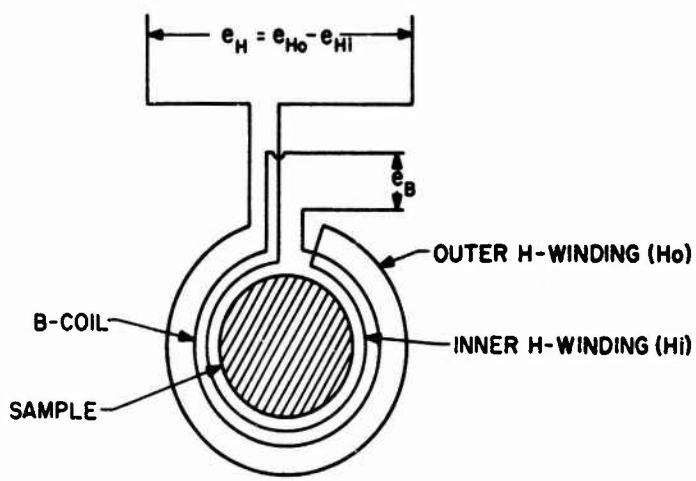

Figure 7. Arrangement of Sensing Coils for Measuring Surface B and H Fields of Rod Samples

The B field is sensed by measuring the flux through the sample with a coil referred to as B coil, which is closely wound to the sample surface. The induced voltage in the B coil is given by

$$e_B = - \frac{d}{dt} [N_B A_S B + N_B (A_B - A_S) H] \tag{12}$$

rearranging

$$e_B = -\frac{d}{dt}[N_B A_S(B-H)+N_B A_B H] \tag{13}$$

where N_B is the number of turns of the B coils, A_S is the cross-sectional area of the sample, and A_B is the average cross-sectional area of a turn of the B winding.

When the B and annular H coils are interconnected in series opposition, we have from Equations (11) and (13)

$$e_{(B-H)} = -\frac{d}{dt}[N_B A_S(B-H)+N_B A_B H-N_H(Ao - Ai)H] \tag{14}$$

If the two coils are balanced such that

$$N_B A_B H = N_H(Ao - Ai)H \tag{15}$$

or

$$N_B A_B = N_H A_H \tag{16}$$

where A_H=(Ao-Ai) is the average annular area between a pair of turns of the H coil, Equation (14) becomes

$$e_{(B-H)} = -\frac{d}{dt}[N_B A_S(B-H)] \tag{17}$$

or

$$e_{(B-H)} = -\frac{d}{dt}[N_B A_S(4\pi M)] \tag{18}$$

and finally after integration

$$e_{(B-H)} = -N_B A_S(4\pi M) \tag{19}$$

The requirement of equal area-turns of the annular H coil and B coil expressed in Equation (16) is very difficult to realize initially in actual coil winding, and it is therefore necessary to arrange the individual windings in such a way that they can be compensated afterwards.

3. ELECTRONIC INTEGRATION

The integration of $\int e_H dt$ and $\int e_{4\pi M} dt$ is performed by two integrating operational amplifiers commonly referred to as Miller integrators. The term, operational amplifier, is a generic term applied to amplifiers whose gain functions are such as to enable them to perform certain mathematical operations such as summation, differentiation, integration, and others. This outstanding versatility of operational amplifiers is obtained from the application of negative feedback. It is recalled from circuit theory that negative feedback in general tends to improve gain stability and linearity, to reduce output impedance, and in some configurations to increase the input impedance. But the extent to which

closed loop performance is improved depends on the magnitude of loop gain (Reference 8). Another useful property of negative feedback which is the basis of all operational amplifier technology is that with enough gain, the closed loop anplifier characteristics become a function of only the feedback components. This can be shown by analyzing the general operational amplifier shown in Figure 8. Applying Kirchhoff's current law to the summing point, yields

$$i_1 = i_i + i_f \tag{20}$$

or

$$(e_1 - e_\epsilon)Y_1 = e_\epsilon Y_i + (e_\epsilon - e_o)Y_f \tag{21}$$

rewrite and solve for e_o:

$$e_o = \frac{e_\epsilon(Y_1 + Y_i + Y_f)}{Y_f} - e_1\frac{Y_1}{Y_f} \tag{22}$$

however, the nominal gain A is defined as

$$A = \frac{e_o}{e_\epsilon} \tag{23}$$

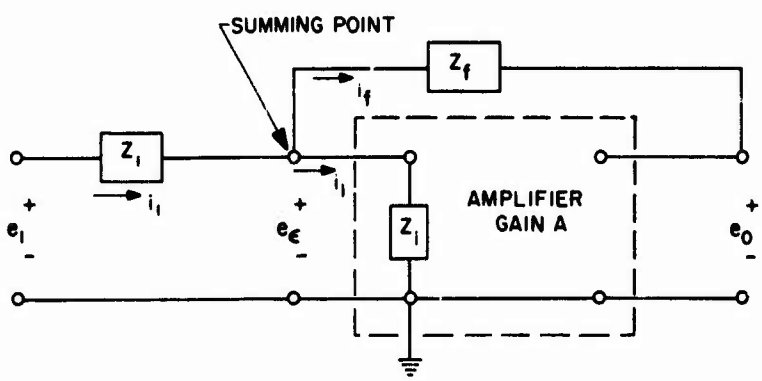

Figure 8. General Operational Amplifier

and the resultant gain with feedback is

$$A_f = \frac{e_o}{e_1} \tag{24}$$

Using these relations in Equation (21) results in

$$A_f = \frac{(Y_1 + Y_i + Y_f)}{Y_f}\,\frac{e_\epsilon}{e_1} - \frac{Y_1}{Y_f} \tag{25}$$

or

$$A_f = \frac{(Y_1 + Y_i + Y_f)}{Y_f}\,\frac{A_f}{A} - \frac{Y_1}{Y_f} \tag{26}$$

solving for A_f

$$A_f\left[1 - \frac{1}{A}\left(\frac{Y_i + Y_1 + Y_f}{Y_f}\right)\right] = -\frac{Y_1}{Y_f} \tag{27}$$

or

$$A_f = -\frac{Y_1}{Y_f}\,\frac{1}{1 - \frac{1}{A}\left(\frac{Y_1 + Y_i + Y_f}{Y_f}\right)} \tag{28}$$

finally:

$$A_f = -\frac{Y_1}{Y_f}\,\frac{1}{1 - \frac{1}{A} - \frac{1}{A}\left(\frac{Y_1 + Y_i}{Y_f}\right)} \tag{29}$$

or equivalently:

$$A_f = -\frac{Z_f}{Z_1}\,\frac{1}{1 - \frac{1}{A} - \left(Z_f\,\frac{Z_1 + Z_i}{Z_1 Z_i}\right)\frac{1}{A}} \tag{30}$$

Since Z_i is always large, $Z_i = 10^{15}\Omega$ in some designs, we may assume infinite input impedance, then

$$A_f = -\frac{Z_f}{Z_1}\,\frac{1}{1 - \frac{1}{A} - \frac{Z_f}{Z_1}\,\frac{1}{A}} \tag{31}$$

so that Equation (31) can be considered an exact expression for the closed loop gain of the general operational amplifier circuit shown in Figure 8. Some important results can be obtained from this expression as will be developed subsequently.

To begin with, let $A \to \infty$ in Equation (31), which then reduces to

$$A_f \approx -\frac{Z_f}{Z_1} \tag{32}$$

This means that as long as e_ϵ is negligibly small (which is implied by $A \to \infty$), the gain is solely dependent on the ratio of the impedances Z_f/Z_1. If Equations (24) and (32) are combined, the resulting expression can be written in the form

$$e_o = -[Z_f Y_1]e_1 \tag{33}$$

This expression is very important, as it contains the explanation of the name "operational amplifier" which has been applied to the circuit of Figure 8.

So far in the development leading to Equation (33) no conditions had been imposed as to the nature of the potentials. Consequently the impedance functions that appear in the equations are functions of the general differential operator p(=d/dt). As a matter of fact, the foregoing development has actually been a manipulation of the controlling differential equation relating the output potential to the input potential, and Equation (33) is the approximate form of this controlling differential equation. If in the special case the applied potential is sinusoidal, then p(=d/dt) is replaced by $j\omega$; Z_f and Y_1 are functions of jw and e_o and e_1 become E_o and E_1, respectively, where E_1 and E_o are the complex amplitudes of the input and output potentials (Reference 9). In this case the steady state relations of Equation (33) is the

$$E_o = - Z_f Y_1 E_1 \tag{34}$$

Equation (32) permits a very convenient approximate circuit to be drawn of the operational amplifier. This approximate circuit is given in Figure 9. The use of the expression "virtual ground" emphasizes the fact that the presence of feedback forces the voltage e_ϵ to zero. This is symbolized by drawing a short from the summing point to ground; no current actually flows through this short, however.

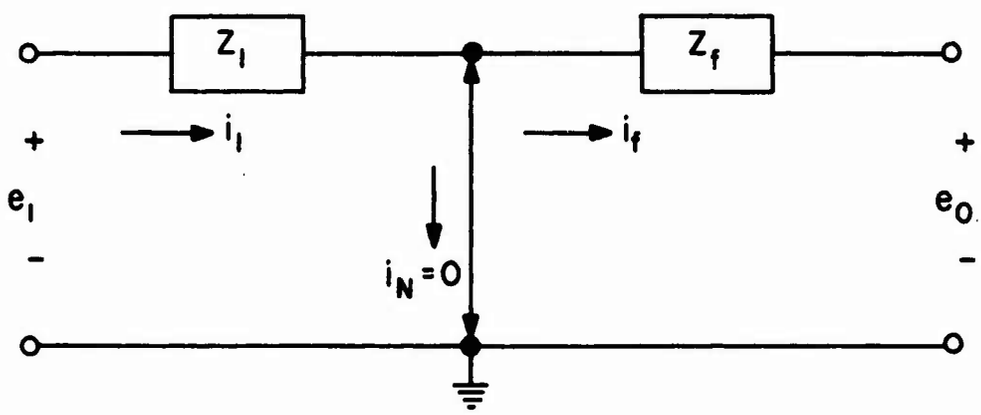

Figure 9. Approximate Equivalent Circuit of Operational Amplifier

If the impedance elements in the circuit of Figure 9 are selected as shown in Figure 10, then $Z_1=R_1$ and Z_f is the operational expression of $Z_f=1/C_f p$, where p(=d/dt) is the time-derivative operator and (1/p) denotes integration with respect to time.

An application of Equation (32) requires that

$$e_o = - \frac{1}{R_1 C_f p} e_1 \tag{35}$$

which is

$$e_o = -\frac{1}{R_1 C_f}\int_0^t e_1 dt \tag{36}$$

This shows that the output potential is related to the integral of the input potential.

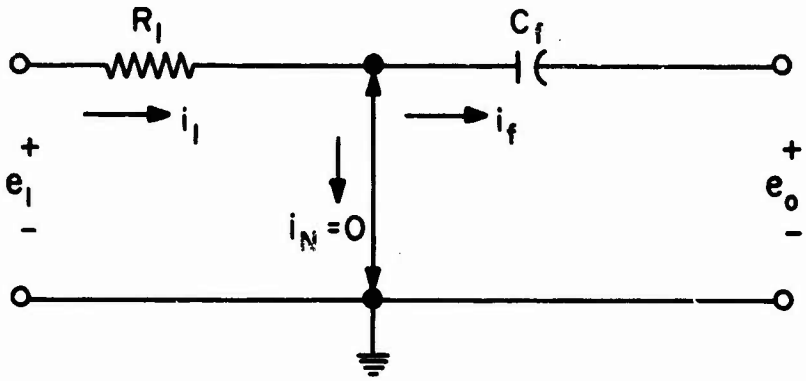

Figure 10. Approximate Equivalent Circuit of Integrating Operational Amplifier

If we substitute $Z_1 = R_1$ and $Z_f = 1/C_f p$ into Equation (31) we obtain

$$A_f = -\frac{1}{R_1 C_f p} \qquad \frac{1}{1 - \frac{1}{A}\left(1 + \frac{1}{R_1 C_f p}\right)} \tag{37}$$

or

$$A_f = \frac{A}{1 + (1 - A)\, R_1 C_f p} \tag{38}$$

Equation (38) becomes then an exact expression for the closed loop gain of the integrating operational amplifier shown in Figure 11.

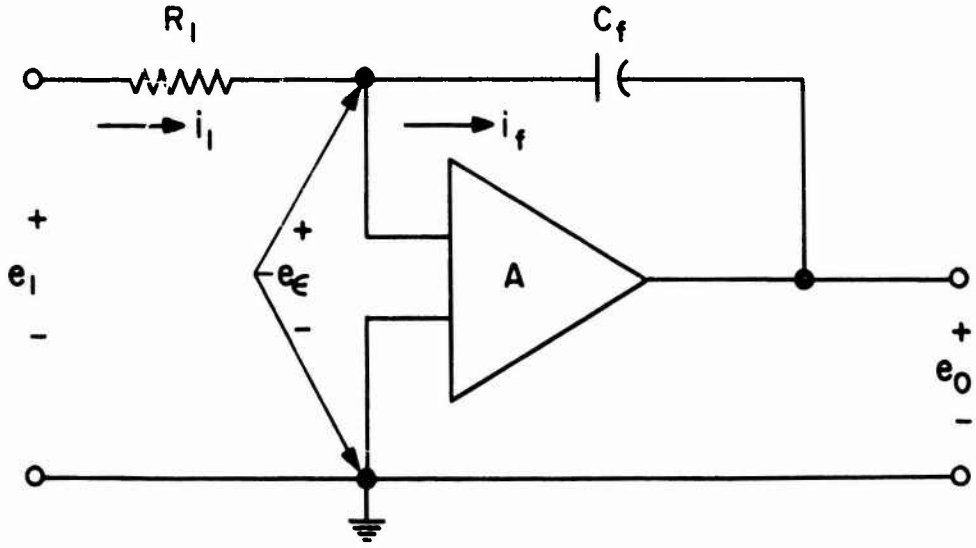

Figure 11. Integrating Operational Amplifier Circuit

Additional insight of operational amplifier characteristics is obtained by considering the current in the feedback element i_f in Figure 11. From inspection of this circuit, i_f is given by

$$i_f = \frac{(e_\epsilon - e_o)}{Z_f} = \frac{e_\epsilon (1 - A)}{Z_f} = \frac{e_\epsilon}{Z_f'} \tag{39}$$

where

$$Z_f' = \frac{Z_f}{1 - A}$$

Obviously, nothing would be changed at the input of the amplifier if the impedance Z_f' were shunted between the summing point and ground, since the same currents would still flow; this is shown in Figure 12.

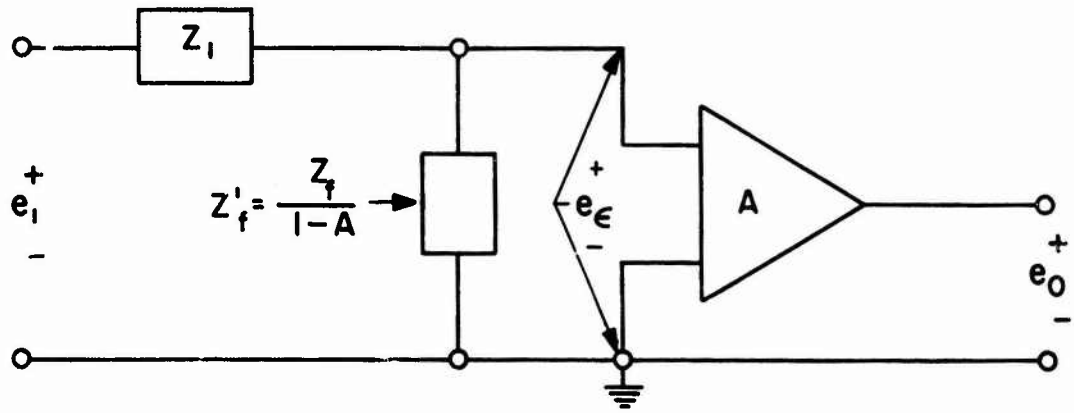

Figure 12. Equivalent Circuit of General Operational Amplifier

The only requirement is that A is known. If we substitute $Z_1 = R_1$ and $Z_f = 1/Cp$ as was done previously, another equivalent circuit of the integrating operational amplifier is obtained as shown in Figure 13. This particular equivalent circuit is extremely useful for calculating the integrator performance. The fact that a capacitor C_f located between the input and output terminals of an amplifier has the same effect on the amplifier as a capacitor $(1-A)C_f$ shunted between input and ground, is known as the Miller effect (Reference 10). It is for this reason that the integrating operational amplifier shown in Figure 11 is often referred to as Miller integrator. The closed loop gain of the Miller integrator shown in Figure 13 is found by recognizing that

$$e_\epsilon = \frac{e_1 \dfrac{1}{C_f p(1 - A)}}{R_1 + \dfrac{1}{C_f p(1 - A)}} \tag{40}$$

or

$$e_\epsilon = \frac{e_1}{1 + (1 - A) R_1 C_f p} \tag{41}$$

and

$$e_o = Ae_\epsilon = \frac{Ae_1}{1 + (1 - A) R_1 C_f p} \tag{42}$$

and finally

$$A_f = \frac{e_o}{e_1} = \frac{A}{1 + (1 - A) R_1 C_f p} \tag{43}$$

which is the same result as that obtained from an analysis of Figure 11; hence circuits shown in Figures 11 and 13 are equivalent.

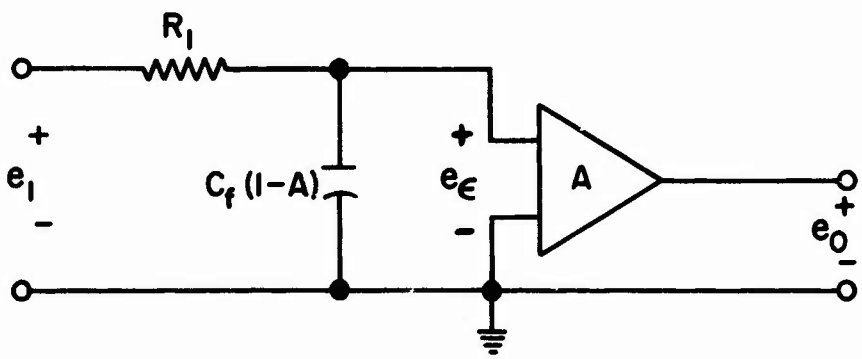

Figure 13. Equivalent Circuit of Miller Integrator

An interesting comparison can now be made between the integrating circuit shown in Figure 14 (Reference 11) and the Miller integrator shown in Figure 13. It is apparent that the input circuit of the equivalent Miller integrator is of the same form as the passive integrator of Figure 14, hence the Miller integrator can be treated as if it were a

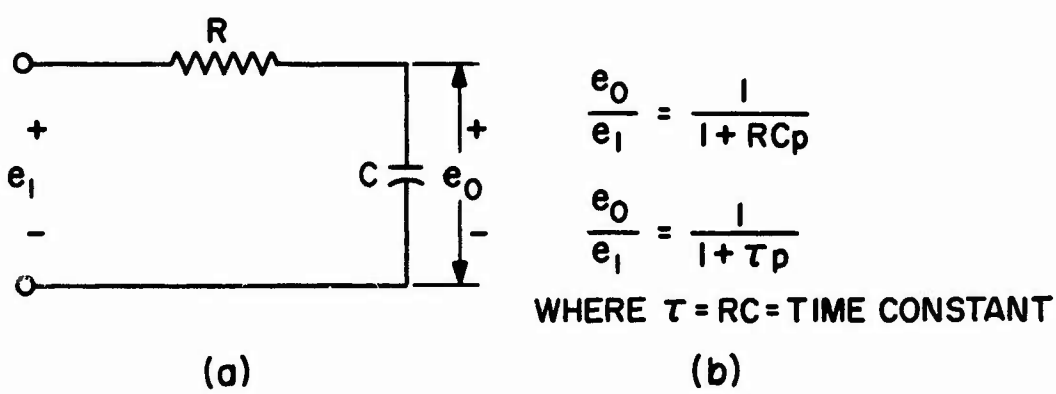

Figure 14. Passive Integrating Circuit

passive integrator. It is also seen that the use of a feedback capacitor, that is the use of a negative feedback, around an operational amplifier has effectively increased the time constant by a factor (1-A) and the same time multiplied the output of the integrating network by the factor A.

4. ANALYSIS OF INTEGRATOR ERROR

If a step input voltage E_1 is applied to the passive integrator of Figure 14, the output response with no initial charge on the capacitor is given by

$$e_o = E_1(1 - e^{\frac{-t}{RC}}) \tag{44}$$

Since the equivalent Miller integrator of Figure 13 is of the same form, we have analogously

$$e_o = A\,E_1(1 - e^{\frac{-t}{(1 - A)R_1C_f}}) \tag{45}$$

or

$$e_o = A\,E_1(1 - e^{\frac{t}{\tau}}) \tag{46}$$

where $\tau=(1-A)R_1C_f$ is the effective time constant of the equivalent Miller circuit. After expansion of the exponential Equation (46) becomes

$$e_o = A\,E_1 \frac{t}{\tau} \left[1 - \frac{t}{2\tau} + \frac{t^2}{6\tau^2} - \cdots\right] \tag{47}$$

It is seen from Equation (47) that the integrator output voltage begins to change linearly with time at a rate equal to AE_1/τ, which corresponds to correct integration of the input step. With increasing integrating time the output voltage deviates more and more from the ramp function given by the first term of Equation (47) and tends to approach AE_1 as a limit

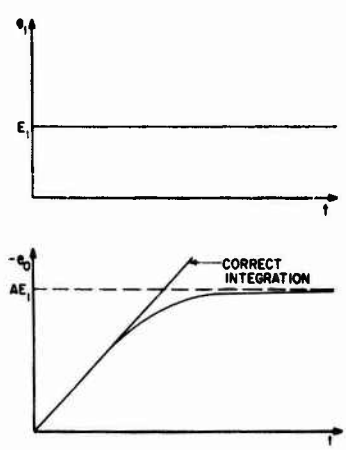

Figure 15. Integration of a Step Function

as shown in Figure 15. It should be noted that the amplifier saturates long before any appreciable deviation from the initial slope occurs, see Section IV. The resulting integrator error is given by the second term of Equation (47). The absolute value of this error is

$$|\epsilon| \leq AE_1 \frac{t^2}{2\tau^2} \tag{48}$$

and the percentage error

$$\epsilon(\%) \leq \frac{\dfrac{AE_1 t^2}{2\ 2}}{\dfrac{AE_1 t}{\tau}} \times 100 \tag{49}$$

$$\epsilon(\%) \leq \frac{t}{2} \times 100 \leq \frac{50\ t}{\tau} \tag{50}$$

So if the integrated output voltage is required to be within ϵ% of the true integral $AE_1 t$, the integration time must be limited to

$$t \leq \frac{\tau}{50} \tag{51}$$

Equation (48) does not account for any errors as a result of stray pickups, drift, and noise which may be introduced at the summing junction or generated within the amplifier.

SECTION IV

DESIGN AND CONSTRUCTION OF THE HYSTERESIGRAPH

1. RECORDER AND AMPLIFIERS

The material presented in Section III forms the basis of the actual design and construction of the instrument. Since the operational amplifiers and the X-Y recorder are purchased parts, the actual design consists basically of determining the integrating networks and the calculation, winding and balancing of the sensing coils. Following this the system can be assembled and its performance checked and compared with the specifications of this application. The X-Y recorder, a Moseley Model 7000 A "Autograf", was already available, and no further consideration is needed. The amplifiers were selected on the basis of large open loop gain, low noise, and low offset. Among the large variety of available types, two Philbrick Model SP 656, chopper stabilized amplifiers having an open loop gain of $|A| = 5 \times 10^7$ were selected for the integrators.

2. DETERMINATION OF INTEGRATING NETWORKS

The noise generated within the amplifier is one of the parameters determining the lower limit of the input signals which may be integrated and amplified. For the amplifiers selected, the noise referred to the input is 10μ Volts peak-to-peak. The minimum input signal which could be tolerated was somewhat arbitrarily set at 100μ Volts.

Assuming a step input to the integrator of 100μ Volts, we have from Equation (47) for correct integration

$$e_o = \frac{A}{(1 - A)RC} \quad e_1(t_2 - t_1)$$

If we let $A/(1-A)RC = 100$ and if the total integration time were 10 seconds, then

$$e_o = 100 \times 0.1 \times 10^{-3} \times 10 = 0.1 \text{ Volts}$$

Since the recorder has 0.5m Volt/inch deflection on the most sensitive range, adequate deflection is assured under these conditions.

An effective gain of 100 can easily be realized by letting R=10K and C=1μf, then

$$A_{eff} = \frac{A}{(1 - A)\ 10^4 \times 10^{-6}} = \frac{100A}{(1 - A)}$$

and since $A=5\times10^7$ and A is negative, then $A/1-A \approx -1$ and $A_{eff} \approx -100$.

The flux linkage sensitivity is determined from a consideration of the magnetic characteristics of the sample and the characteristics of the electromagnet in which the samples are tested. From Faraday's law of induction

$$e = -N\frac{d\phi}{dt} \times 10^{-8} \quad \text{Volts} \tag{2}$$

Since $d\phi/dt$ depends on how fast the applied field is changed from $H_{max}(+)$ to $H_{max}(-)$. A minimum time of 10 seconds was considered a realistic value, consistent with the inductance-limited reversal time of the electromagnet and the response of the recorder, then from Equation (2)

$$e\Delta t = -N\Delta\phi \times 10^{-8} \quad \text{Volt-sec}$$

or

$$edt = -Nd\phi \times 10^{-8} \quad \text{Volt-sec}$$

Using the minimum voltage of 100μ Volts as determined before, the equivalent flux linkage sensitivity is then

$$0.1 \times 10^{-3} \times 10 = 1 \text{ m Volt-sec}$$

Assuming a coil of 500 turns, the equivalent flux change which is measurable with sufficient accuracy is then

$$\Delta\phi = \frac{1 \times 10^{-3}}{500} = 2\mu\text{Volt-sec} = 2 \times 10^{-6} \text{ Weber}$$

From the specifications of Section I, the minimum saturation value for the magnetic portion of the sample is approximately $4\pi M_s = B_s =$ 6000 Gauss, and the typical packing fraction is 5%. The latter can be taken into account for the purpose of this calculation by assuming that we deal with a sample having the full saturation value of the massive magnetic material, but a cross section of only 5% of the actual composite area, hence

$$A_s' = \frac{5}{100} \times A_s = \frac{5}{100} \times \frac{\pi}{4} \quad (1.1\text{cm})^2 = 0.048\text{cm}^2$$

The peak-to-peak flux change is then

$$\Delta\phi = 2\phi_s = 2A_s' \times B_s = 2 \times 0.048 \times 6 \times 10^3 = 575 \text{ Maxwell} = 5.75 \times 10^{-6} \text{ Weber}$$

Comparing this value with the theoretical value obtained from the amplifier characteristics, it is seen that a flux linkage sensitivity of 1m Volt-sec is more than adequate to measure $4\pi M_s$ of low induction materials.

To measure peak-to-peak values of $_M H_c$=100 Oe at applied fields of H_{max}=15,000 Oe, assume an area for the annular H coil of 1.8 cm^2, then

$$\Delta\phi = 2\phi_{max} = 2 \times 1.8 \times 15 \times 10^3 = 54 \times 10^3 \text{ Maxwell}$$

or

$$= 5.4 \times 10^{-4} \text{ Weber}$$

Since the flux change as seen by the H channel is about 100 times that obtained c he 4πM channel for the dilute samples, an effective gain of 10 was considered adequate. The corresponding values of R and C were found to be R=100 KΩ and C=1μf.

3. INTEGRATOR PERFORMANCE

Each integrating amplifier was calibrated by applying a known step input voltage to the amplifier input. The amplifier output was connected to the Y-axis of the recorder. The X-channel of the recorder was operating in the sweep mode, which was set at 100 sec/inch. A step input $E_{in}(+)$=0.59m Volts was applied while the amplifier was saturated at $V_{sat}(-)$. With the recorder turned on, the integration time was measured from the time the amplifier became unsaturated. After the amplifier reached $V_{sat}(+)E_{in}$ was reversed until the amplifier reached $V_{sat}(-)$ again. One such cycle is shown on the graph of Figure 16. On the up-scale integration, the integration time was found to be

$$t = 432 \text{ sec}$$

the calculated output for correct integration

$$E_o = AE_{in}t = (100)\ (0.59 \times 10^{-3})\ (432) = 25.48 \text{ Volts}$$

measured output from Figure 16

$$E_o = 25.5 \text{ Volts}$$

On the down-scale integrat on the integration time was found to be

$$t = 427 \text{ sec}$$

and the calculated output for correct integration

$$E_o = (100)\ (0.59 \times 10^{-3})\ (427) = 25.20 \text{ Volts}$$

the measured output from Figure 16

$$E_o = 25.5 \text{ Volts}$$

While on the up-scale integration the integrating error is <0.01%, on the down-scale integration this error is approximately 1%.

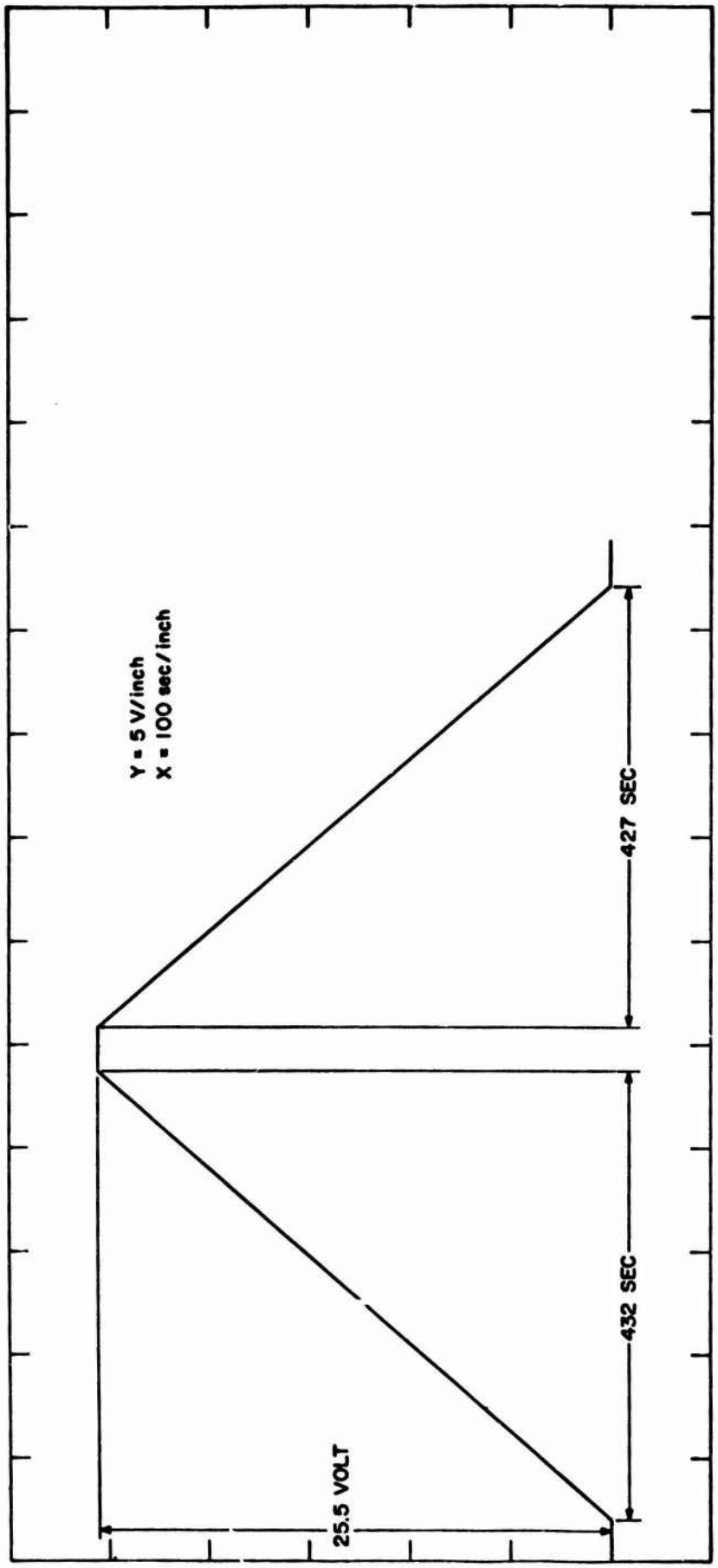
Y = 5 V/inch
X = 100 sec/inch
427 SEC
432 SEC
25.5 VOLT

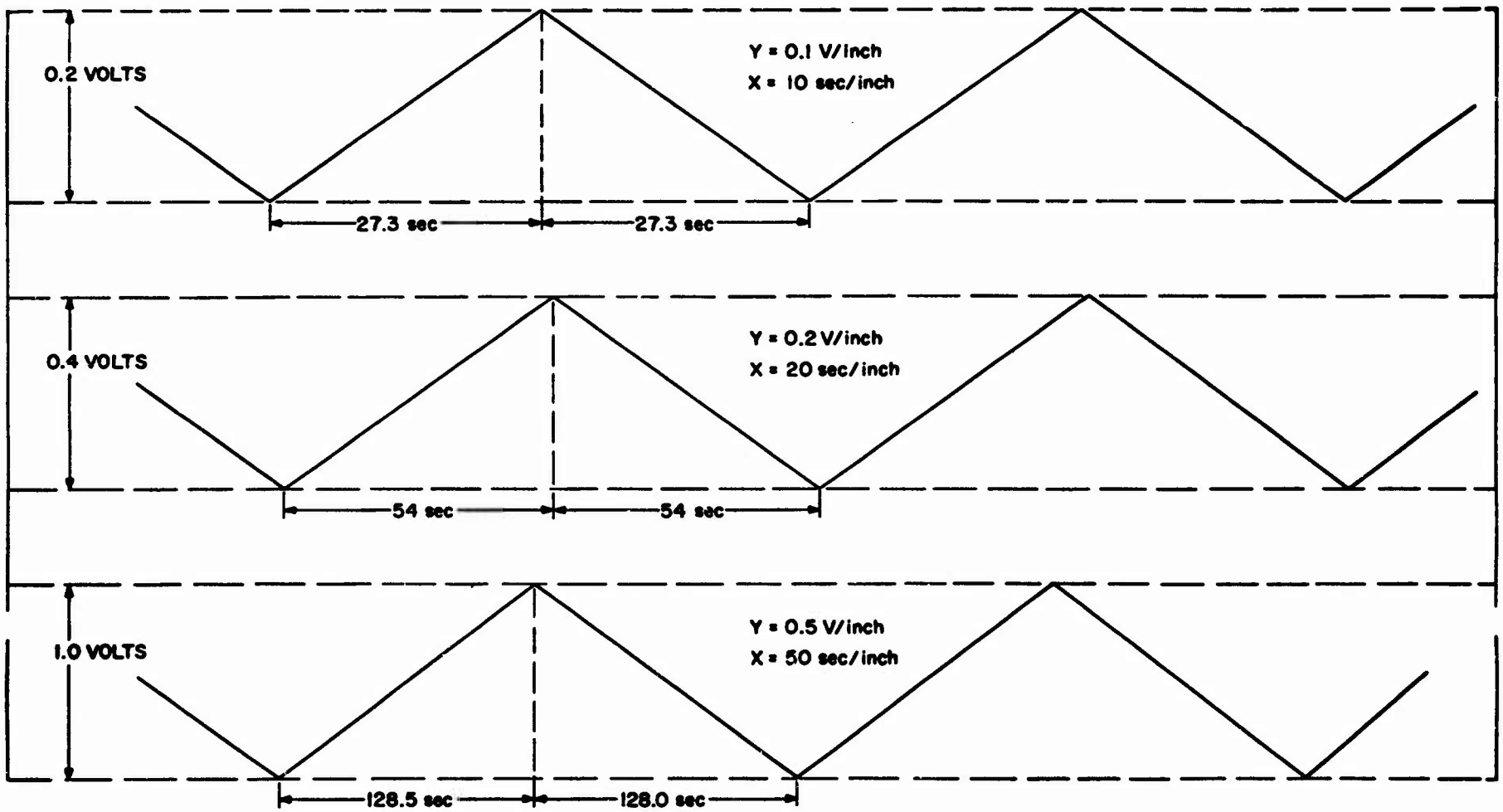

Figure 17. Response of Miller Integrator to Step Input (Short Time Integration)

This performance was considered quite satisfactory since it takes approximately 1 minute for plotting one complete $4\pi M$ versus H loop, after which the integrator is reset. Figure 17 shows the response of one of the integrators to the same step input voltage but with different sweep speeds. Again the observed integrating error is negligibly small.

According to Equation (51) the theoretical integration time should be equal to or less than 1000 sec for an integration error of 0.1%. The deviation from this theoretical result must be attributed to drifts and noise in the amplifier.

4. COIL CONSTRUCTION

In Section III we saw that the criteria for obtaining a voltage proportional to $4\pi M$ from the annular H coil and the B coil was expressed by the relation

$$N_B A_B = N_H A_H$$

where $A_H = (A_o - A_i)$ is the average area of the annular H coil. This equation is difficult to satisfy because of rather large and unpredictable discrepancies which exist between the calculated area-turns of a coil and the area-turns obtained after the coil has been wound. It is therefore necessary to arrange the individual windings which make the annular H coil and B coil in such a way that the area-turns of one coil can be precisely adjusted to satisfy Equation (52). Since Equation (52) requires also that the number of turns of the H_o and H_i windings are equal, the annular H coil was chosen to be the coil whose individual turns as well as area-turns could be adjusted after completion of winding.

A winding arrangement which could serve these purposes is shown schematically in Figure 18. In this schematic the H_i winding is wound on the bobbin core, followed by the B and H_o windings respectively. The bottom layer of the H_i winding and the top layer of the H_o winding are provided with additional turns which serve as the pull turns for compensation purposes.

The physical dimensions of the bobbin were determined from the sample size, the number of turns and layers for a predetermined winding length and are shown in Figure 18. In order to obtain adequate signal output from the coils, 500 turns for each of the three windings were chosen on the basis of the calculations in Section IV. The free winding length was chosen to be 1/3 of the sample length. This was the best compromise between the desired number of turns and a manageable wire size.

The H_i and H_o windings were wound with #42 AWG Formvar wire and the B winding with #38 AWG Formvar. The following winding data

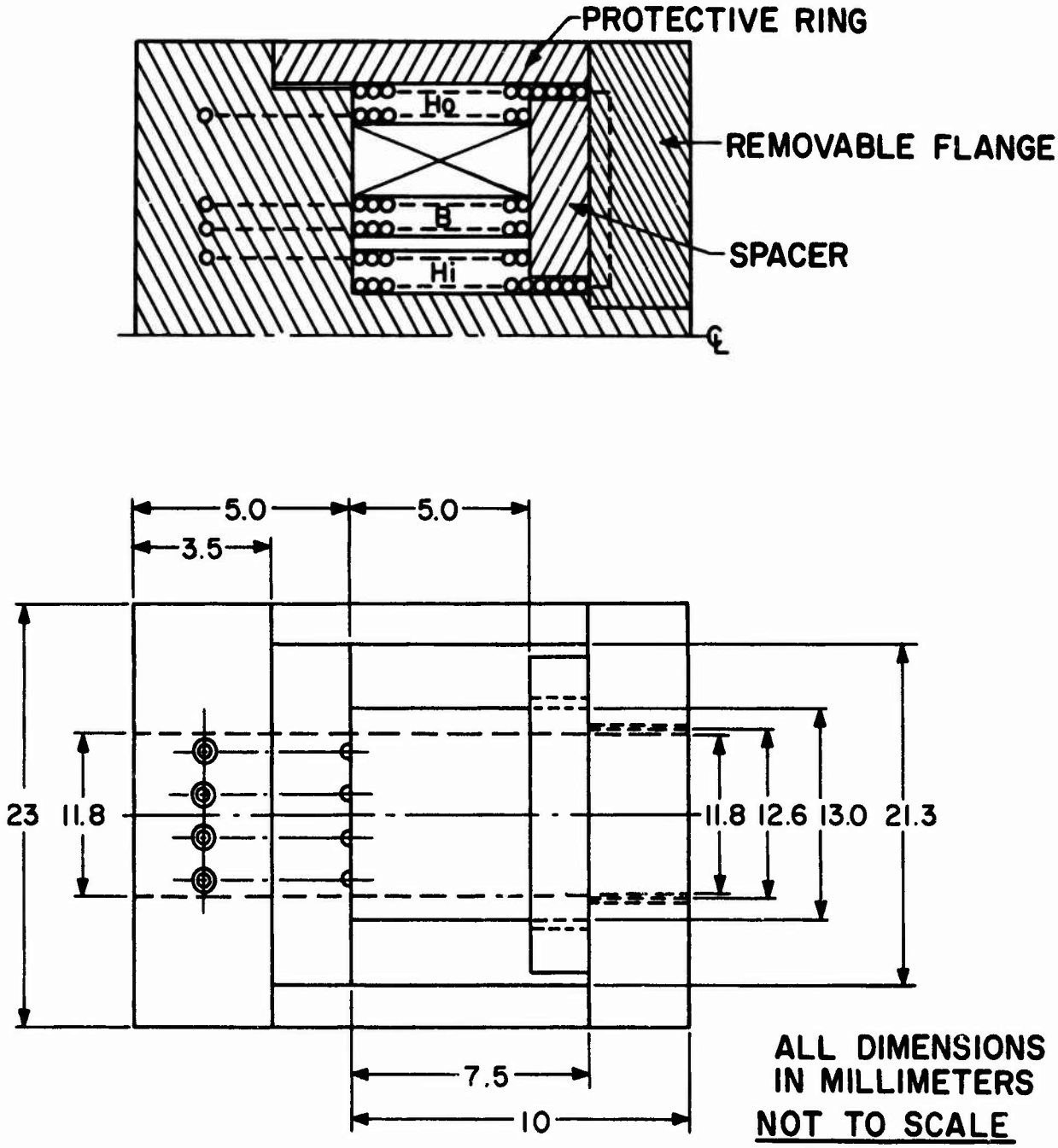

Figure 18. (a) Cross Section of Coil Arrangement
(b) Coil Form

were obtained while actually winding the coils according to Figure 18:

Inner H winding H_i:

total number of turns	N_{Hi}	=	480
inside diameter	D_i	=	13.0 mm
outside diameter	D_o	=	14.0 mm
average diameter	D	=	13.5 mm

B winding:

total number of turns	N_B	=	470
inside diameter	D_i	=	14.0 mm
outside diameter	D_o	=	17.5 mm
average diameter	D_B	=	15.8 mm

Outer H winding H_o:

total number of turns	N_{Ho}	=	480
inside diameter	D_i	=	20.1 mm
outside diameter	D_o	=	21.1 mm
average diameter	D	=	20.6 mm

The effective area of the B winding is then

$$A_B = \frac{\pi}{4} D_B^2 = .785 \times 1.58^2 = 1.97 cm^2$$

5. COIL COMPENSATION

After the coil was wound the detachable flange was removed from the coil form and the pull ends of the individual H windings were joined together to form the annular H coil. The coil was then checked for unbalance at the center of a long solenoid and subjected to a 420 Hz ac-field having H_{max} = 67.5 Oe. The initial unbalance between the annular H coil and the B coil was found by measuring e_B and e_H individually and e_{B-H} directly. The RMS values of these voltages were E_B = 1.18 Volts, E_H=1.21 Volts and $E_{(B-H)}$=28.2 m Volts. Since E_H

exceeds E_B by 28.2 m Volts or 2.3% the excess number of H turns was found as

$$\text{excess } N_H = \frac{2.3 \times 480}{100} = 11.0 \text{ turns}$$

After pulling 10 annular turns, $E_{(B-H)}$ was measured again, giving $E_{(B-H)} = 0.68$ m Volts. Because of obviously present stray-pickup voltages no further improvement was expected by this method. Instead the coil was placed in the electromagnet and the compensation was checked in a slow changing dc-field using the hysteresigraph. Without a magnetic sample in the coil, $E_{(B-H)} = E_{4\pi M} = 0$ and for a perfectly balanced coil, the X-Y recorder should draw a straight line while the applied field is changing. By setting the X-axis attenuator (H-channel, $A_{eff}=10$) to 0.2 V/inch and the Y-axis attenuator (4πM-channel $A_{eff}=100$) to 0.02 V/inch, the 4πM-channel is then 100 times as sensitive as the H-channel. Under these conditions any remaining unbalance of equal area-turns is precisely readable on the X-Y plot. The result is as shown in Figure 19.

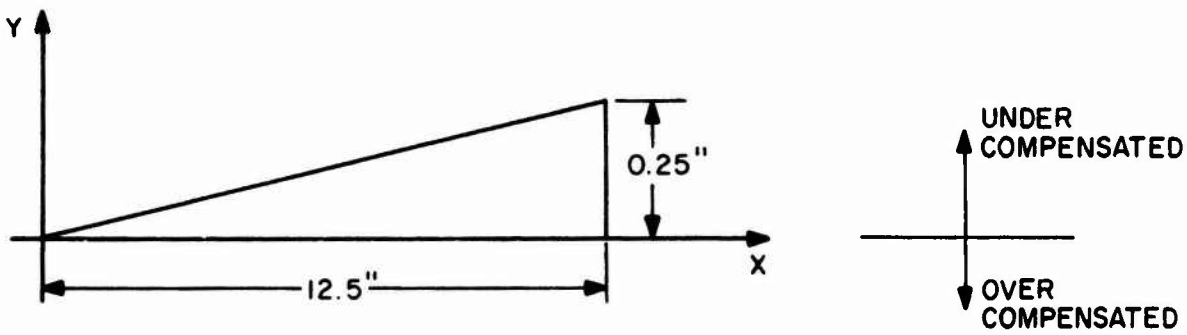

Figure 19. Remaining Coil Imbalance

The error in area turns as obtained from the hysteresigraph is then

$$\delta_{NA} = \frac{0.25}{12.5 \times 100} \approx 0.02\%$$

With N_B=470 turns this apparent error amounts to

$$\delta_{NA} = 0.0002 \times 470 \approx 0.1 \text{ annular turn}$$

This compensation for equal area turns of the B and H coils was considered satisfactory and no further improvements were attempted.

The area of the B coil can now be determined by placing the coil again in the same ac-field of the solenoid as before. The voltage induced

in the B coil by an ac-field is given by

$$E = 4.44 \times f \times N_B \times \phi_{max} \times 10^{-8} \quad \text{Volts} \qquad (53)$$

Since no iron is involved here, $\phi_{max} = A_B x H_{max}$ and substituting numbers in Equation (53), we have

$$1.18 = 4.44 \times 420 \times 470 \times A_B \times 67.5 \times 10^{-8}$$

if this expression is solved for A_B the result is

$$A_B = \frac{1.18}{.592} = 1.99 \text{ cm}^2$$

By comparing the value for the area of the B coil obtained from the physical coil dimensions with that obtained from the ac measurement, it is seen that they are in good agreement. Since the annular H coil and the B coil are balanced with an error of approximately 0.02% the area of the H coil is then, $A_H = 1.99 \text{ cm}^2$ also.

To protect the coil from damage in everyday use, the coil was inserted into a holding fixture and sealed on both ends with epoxy, see Figure 21.

The entire system was then wired according to the schematic shown in Figure 20.

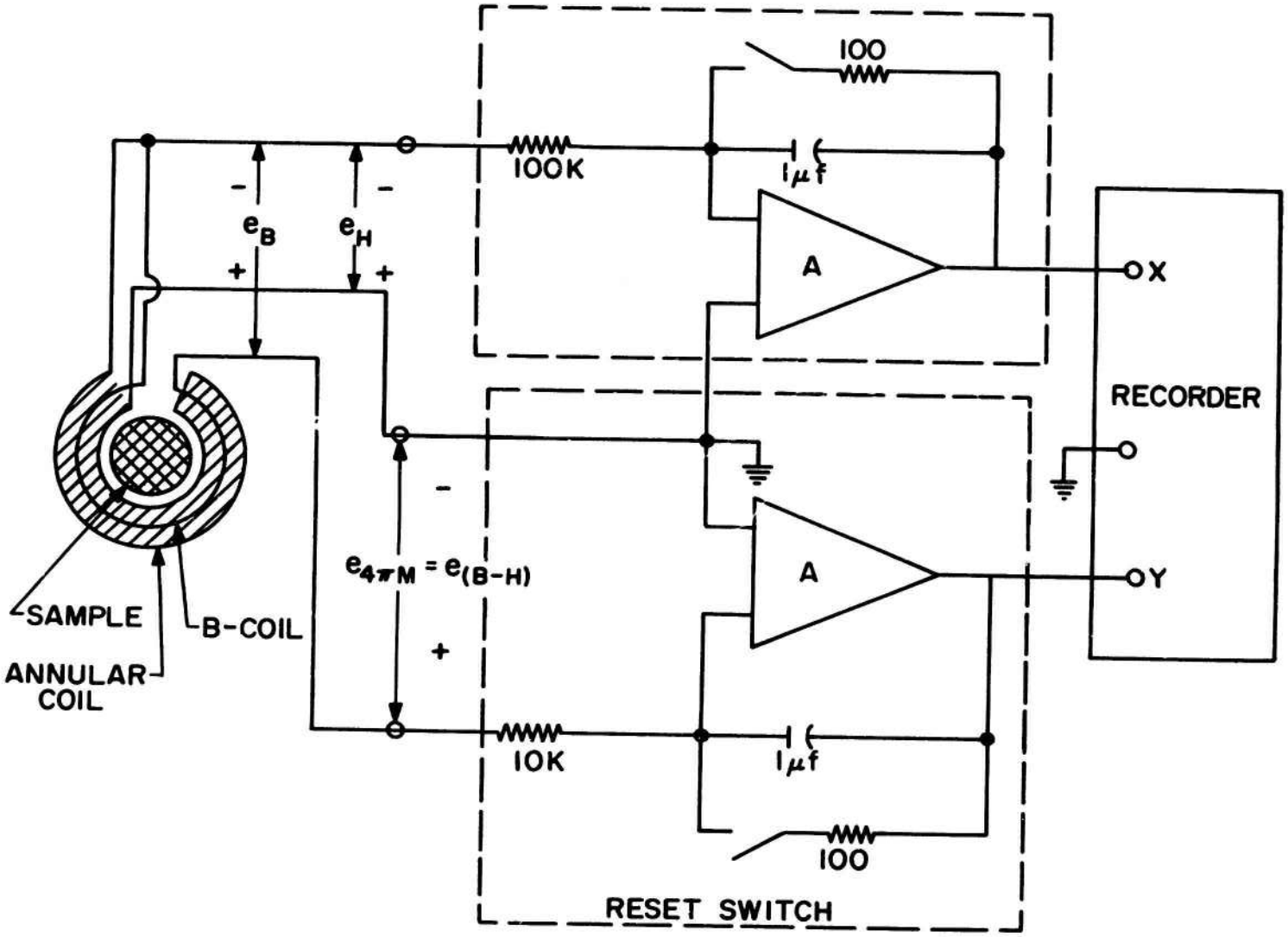

Figure 20. Schematic of Hysteresigraph

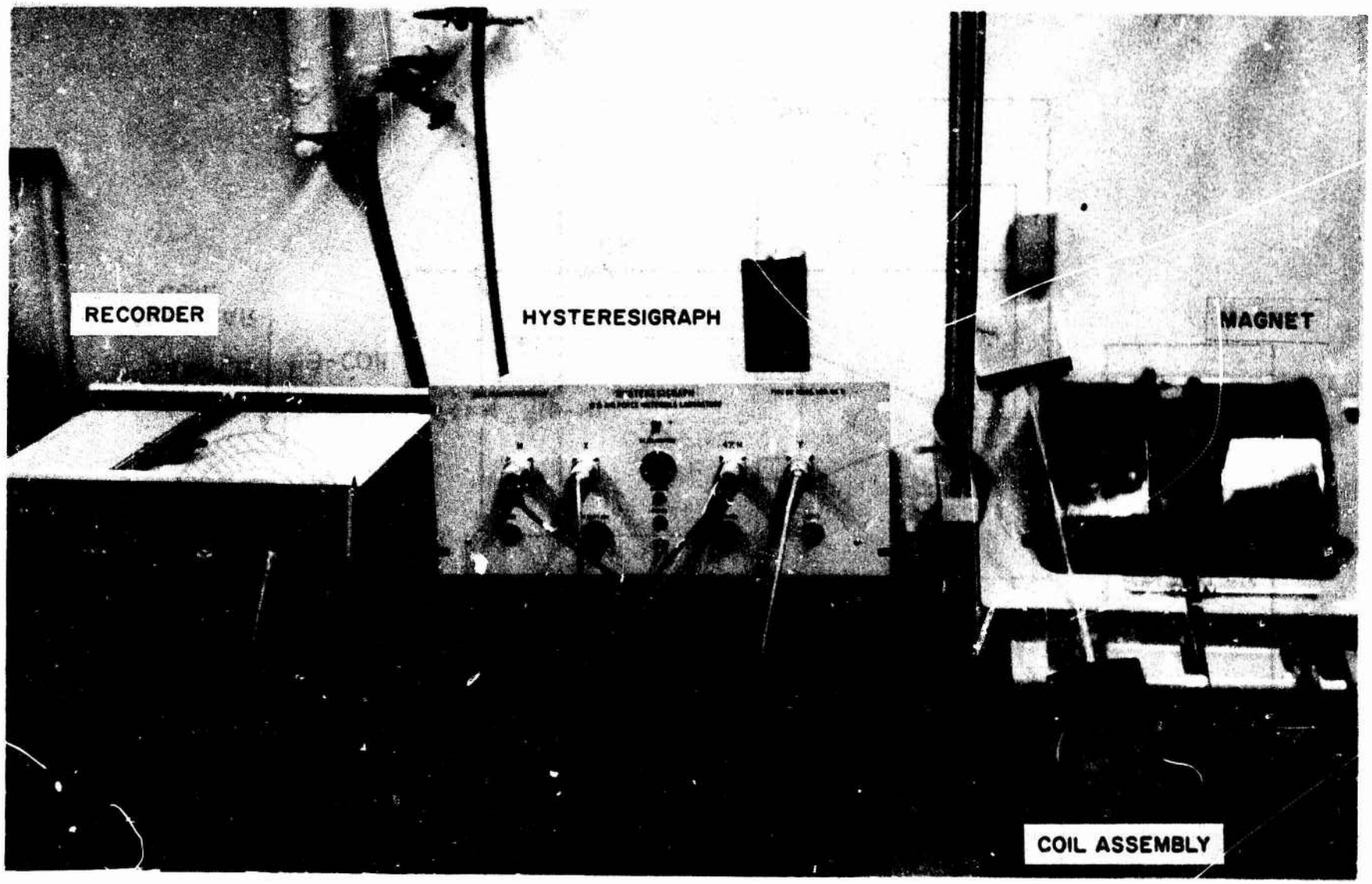

Figure 21. Magnet and Hysteresigraph Set Up for Testing

SECTION V

CALIBRATION OF THE HYSTERESIGRAPH

1. CALIBRATING PROCEDURE

The calibrating procedure of the completely interconnected hysteresigraph consists of separately calibrating the H and (B-H) coils. The calibration of the H coil was derived from the known applied field between the pole caps of the electromagnet. The calibration of the (B-H) coil was derived from the known saturation magnetization $4\pi M_s$ of a standard test sample of pure iron.

2. CALIBRATING THE H COIL

A Rawson rotating coil Gaussmeter was used to measure the applied field between the pole caps of the electromagnet which were separated by a distance equal to the coil length. The electromagnet was then excited and cycled several times through a maximum field of either polarity. The maximum field excursions in both the positive and negative directions were recorded and averaged out to get the peak-to-peak applied field. Without changing the pole separations nor the exciting magnet current, the Gaussmeter probe was now replaced by the coil assembly without a test sample and the magnet was again cycled. Since it is under these conditions $4\pi M=0$, the hysteresigraph will then draw a straight line along the X-axis, which is now a measure of the peak-to-peak applied field.

From the Rawson Gaussmeter the measured peak-to-peak field was

$$H_{p-p} = 33,100 \text{ Oe}$$

With the coil in the magnet and the recorder sensitivity set at X=0.2 V/inch a line 14.67" length was obtained as shown on Figure 22. The calibration constant for the H field is now

$$C_H = \frac{33,100}{14.67 \times 0.2} = 11,280 \left[\frac{\text{Oe}}{\text{Volt}}\right]$$

This completes the calibration of the H coil.

3. CALIBRATING THE (B-H) COIL

The (B-H) coil was calibrated by recording hysteresis loops of a pure iron standard of accurately known dimensions and saturation magnetization value. The number used for the latter is $4\pi M_s$=21,510 Gauss. It was determined at the Air Force Materials Laboratory on

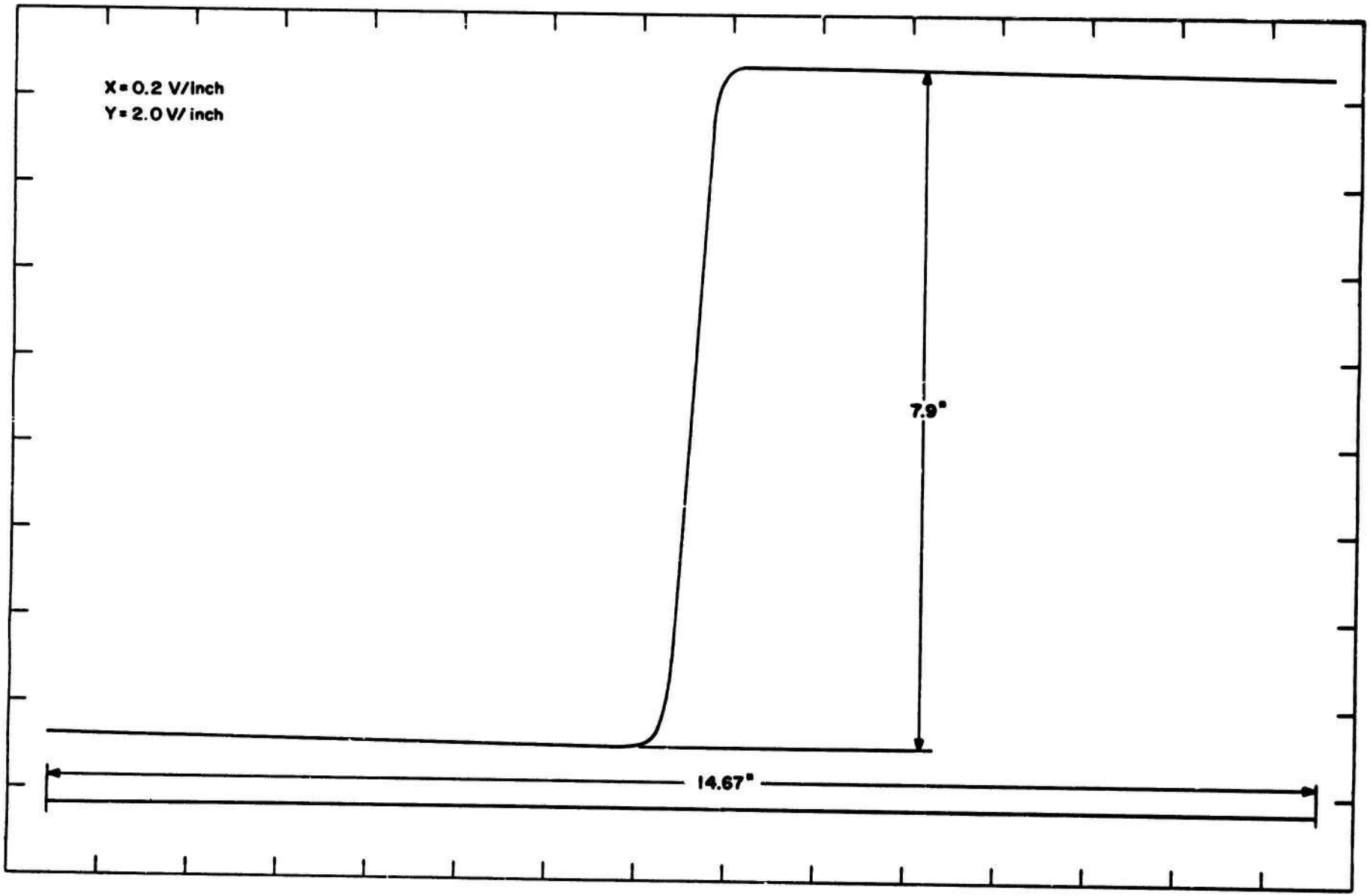

Figure 22. Coil Calibration Curves

iron from the same piece, using a pull coil technique and fields up to 50 kOe (Reference 12). This number is considered more accurate than the often used literature value of $4\pi M_s$=21,580 (Reference 13). Placing this sample into the coil and cycling the applied field as described above resulted in the $4\pi M$ versus H plot shown in Figure 22. The Y-sensitivity of the recorder was set at 2 Volts/inch and the measured distance between the lines representing the peak-to-peak magnetization ($2 \times 4\pi M_s$) as found from Figure 19, was d_M=7.9 inches. The calibration constant for the $4\pi M$ - channel can now be determined as

$$C_{4\pi M} = \frac{2 \times 21,510}{7.9 \times 2} = 2720 \left[\frac{\text{Gauss}}{\text{Volt}}\right]$$

If a sample under test has a cross-sectional area A_s' different from the cross-sectional area A_s of the iron standard, the new magnetization constant is then

$$C'_{4\pi M} = \frac{C_{4\pi M}}{\frac{A_s'}{A_s}} \left[\frac{\text{Gauss}}{\text{Volt}}\right]$$

where A_s is the cross-sectional area of the standard.

For the test samples used here, A_s'=1.00 cm^2 hence,

$$C'_{4\pi M} = \frac{2720}{\frac{1.000}{0.882}} = \frac{2720}{1.132} = 2400 \left[\frac{\text{Gauss}}{\text{Volt}}\right]$$

This completes the calibration of the (B-H) coil.

4. OVERALL ACCURACY

The accuracy of the instrument is determined by the accuracy of the quantities which were used for its calibration. The accuracy of $4\pi M_s$ of the high purity iron sample is estimated at a few tenths of 1%. The accuracy of H is determined by the $\pm$ 1% accuracy of the Rawson rotating coil Gaussmeter. The overall accuracy of the entire hysteresigraph is then estimated at about 1%.

SECTION VI

OPERATION OF THE HYSTERESIGRAPH

The only preliminary work prior to drawing $4\pi M$ versus H loops consists of eliminating the drift by means of the offset adjustment provided for each amplifier. An initial warm-up period of about 20 minutes is required to stabilize the amplifier outputs before these adjustments can be made. Thereafter only occasional readjustments are necessary. Following this procedure and with the coil and sample positioned between the pole caps, the magnet can now be excited. Before bringing the recorder pen into writing position, the applied field is cycled several times to allow adjustment of the proper $4\pi M$ [illegible] scales on the recorder attenuator. Upon completion of a f[illegible]ial cycles, the integrating capacitors are discharged and the pen is brought into writing position, and the $4\pi M$ versus H loops can be recorded.

Once a complete loop is drawn the coordinate axis can be established and $4\pi M_r = B_r$ and ${}_MH_c$ can be evaluated using the calibration constants given in Section V. Examples of drawn $4\pi M$ versus H loops are shown in Figures 23 through 25.

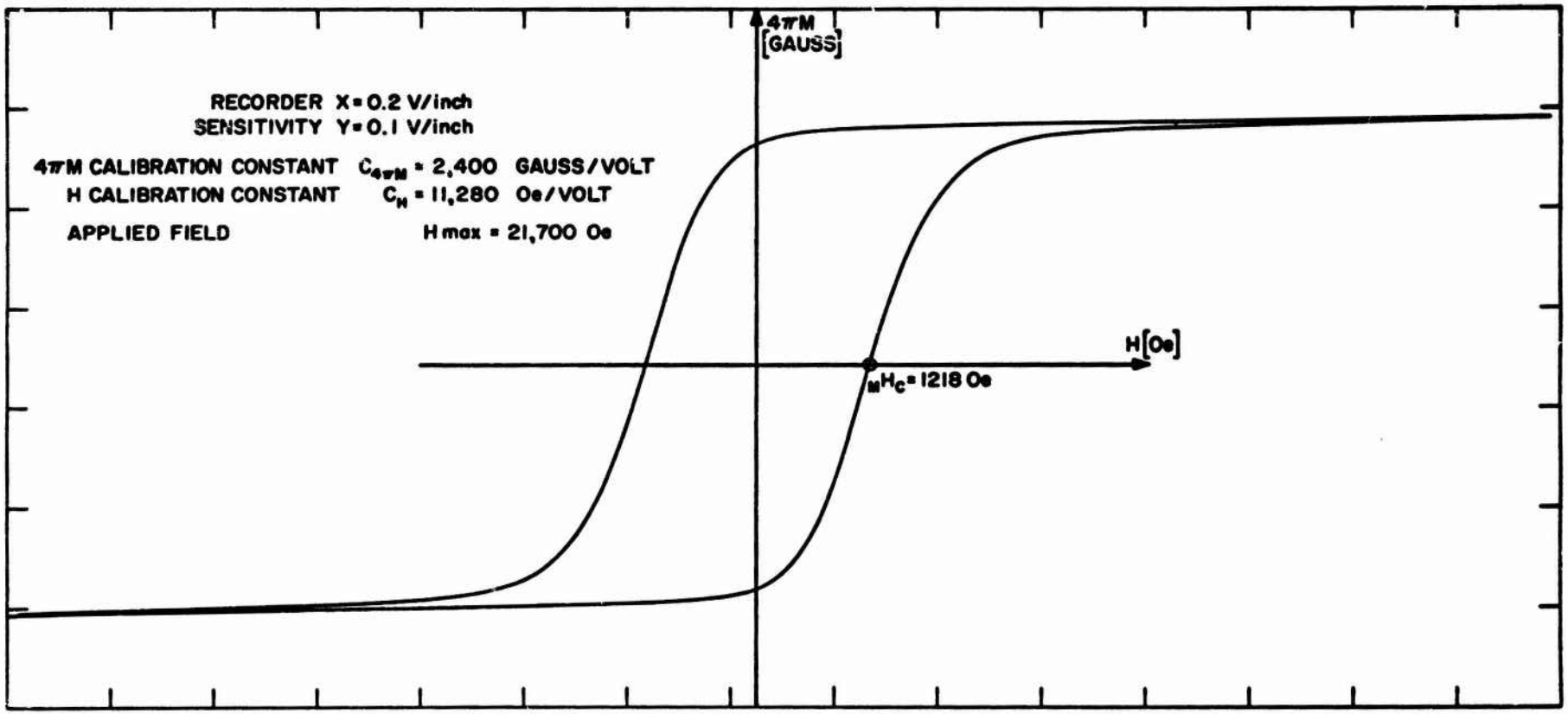
4πM
[GAUSS]
RECORDER X = 0.2 V/inch
SENSITIVITY Y = 0.1 V/inch
4πM CALIBRATION CONSTANT $C_{4\pi M}$ = 2,400 GAUSS/VOLT
H CALIBRATION CONSTANT C_H = 11,280 Oe/VOLT
APPLIED FIELD H max = 21,700 Oe
H[Oe]
$_MH_C$ = 1218 Oe

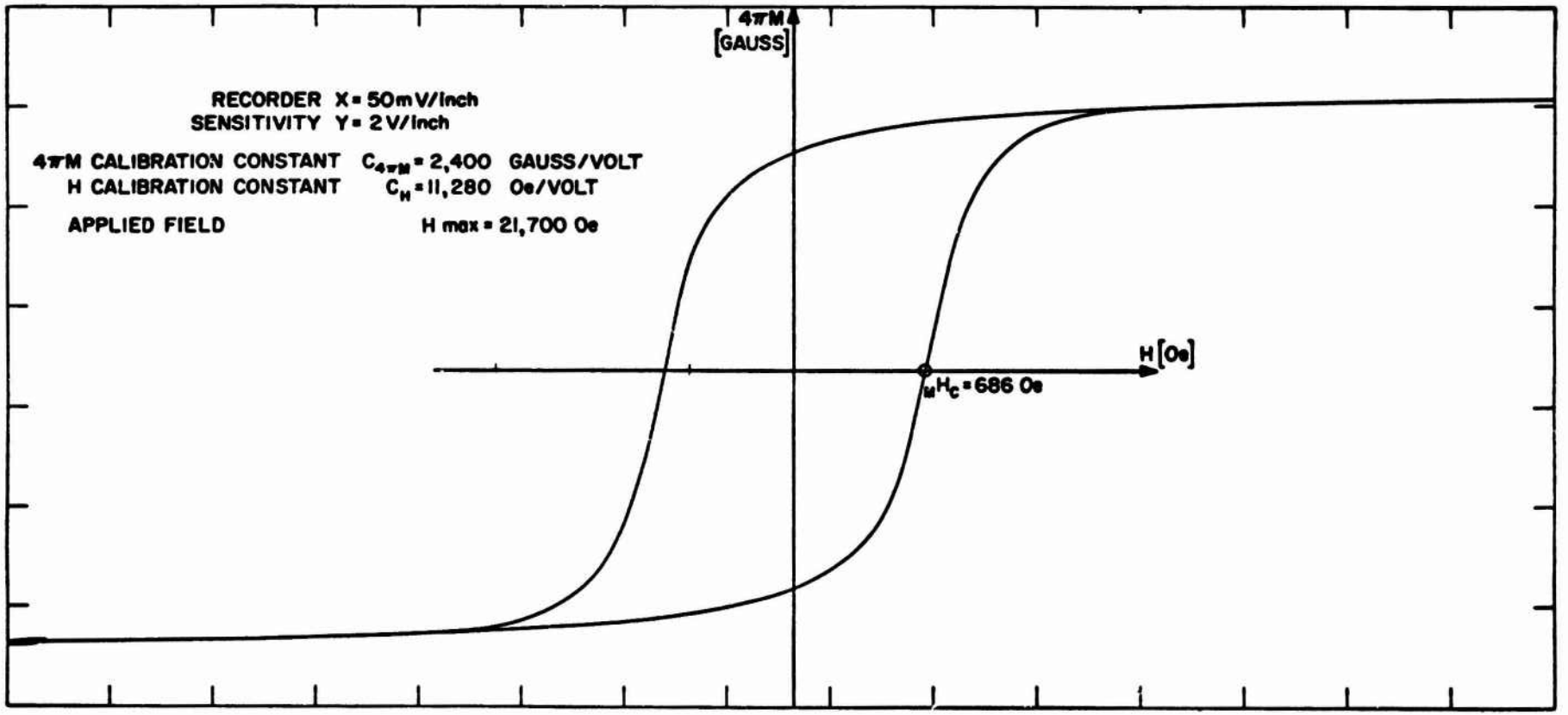

Figure 24. 4πM Versus H Loop of a Typical Alnico VI Sample

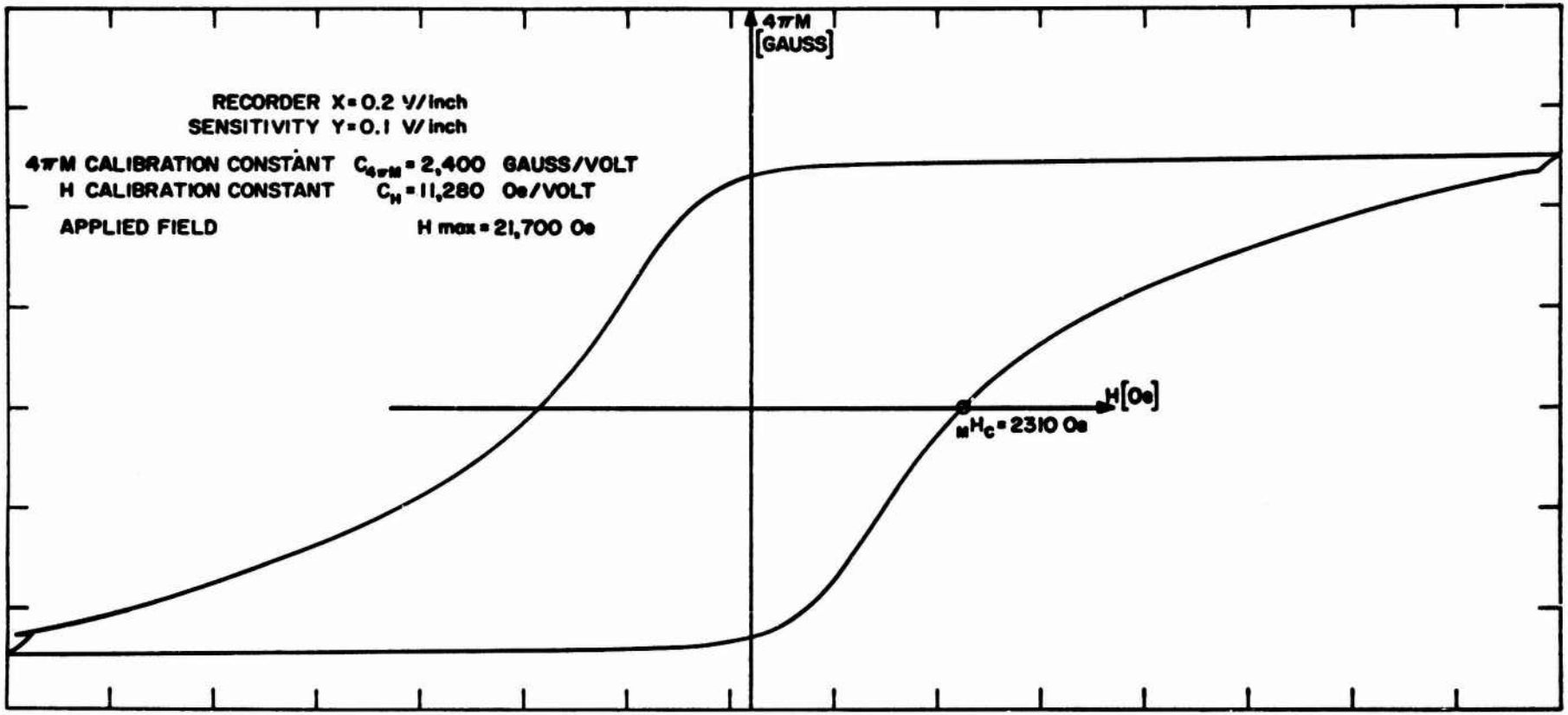

Figure 25. 4πM Versus H Loop of a Typical $SmCo_5$ Sample

SECTION VII

SUMMARY

1. SIGNIFICANCE OF THIS CONTRIBUTION

The hysteresigraph described in this paper was designed to plot $4\pi M$ versus H loops of dilute fine particle permanent magnets. As such, this instrument has made valuable contributions toward the evaluation of magnetic properties of materials.

The fact that specialized instruments of this nature are not available on the commercial market places the burden on the individual investigator to design and build his own test equipment. To assist other investigators in this field, this paper has been presented as a case study of a hysteresigraph design. The novel feature of this particular instrument is the coil arrangement which allows the measurement of the B - and H fields at the surface of cylindrical samples. As a result the instrument described here is not limited to drawing $4\pi M$ versus H loops, but can also be adapted to plot B versus H loops of cylindrical samples. Among all hysteresigraphs which have come to the attention of the writer, only the one reported by Cioffi (Reference 1) can be used to plot B versus H loops of rod samples. However, the technique used there is quite different and much more involved than the one used here. In addition, the instrument described here uses only "off the shelf" items, with the exception of the coil. The necessary flexibility for designing an instrument for a particular application is thus preserved.

The main objective of this particular application was the evaluation of ${}_MH_c$ of large numbers of fine particle permanent magnets. This objective has been accomplished quite satisfactorily, since over 200 samples have been tested thus far without difficulties.

2. RECOMMENDATIONS FOR FURTHER STUDY

Experience with this instrument has shown that further studies are needed toward the improvement of long-time electronic integration. As was shown in Section IV, accurate integration is possible over time periods of 7-10 minutes. This performance was more than adequate for this application. However, more and more magnetic testing of hard magnetic materials is being done in superconducting solenoids which require up to 30 minutes or more to finish one complete cycle. For this reason hysteresigraphs of the type discussed here or in the literature cannot be used with superconducting solenoids. In this latter application, the sample sizes can be only a small fraction of the ones used at the Air Force Materials Laboratory, thus necessitating much smaller

sensing coils. Additional studies are therefore required regarding the sensitivity requirements.

3. FUTURE USE

The development of the instrument described here has closed an existing gap in the available types of hysteresigraphs. It is hoped that this instrument can serve as a basis for further developments leading to an extension of its use to magnetic testing in superconducting solenoids.

BIBLIOGRAPHY

1. P. P. Cioffi, "A Recroding Fluxmeter of High Accuracy and Sensitivity", Review of Scientific Instruments, vol. 21, number 7, pp. 624 - 628, July, 1950.

2. P. F. Elarde, "All Electronic Magnetic Hysteresigraphs", The Western Electric Engineer, pp. 8-14, January, 1965.

3. R. R. Bockemuehl and W. E. Sargeant, "Practical Hysteresigraphs", Journal of Applied Physics, supplement to vol. 31, number 5, pp. 180 S-182 S, May, 1950.

4. P. Mazzetti and P. Soardo, "Electronic Hysteresigraph Holds dB/dt Constant", Review of Scientific Instruments, vol. 37, number 5, pp. 548-552, May, 1966.

5. K. J. Strnat and G. I. Hoffer, YCo_5, A Promising New Magnetic Material, AF Technical Report AFML-TR-65-446, May, 1966.

6. E. W. Golding, Electrical Measurements and Measuring Instruments, Sir Isaac Pitman Publishing Co., London, 1941.

7. E. M. Pugh and E. W. Pugh, Principles of Electricity and Magnetism, Addison-Wesley Publishing Co., Reading, Mass., 1962.

8. J. Millmann, Vacuum Tube and Semiconductor Electronics, McGraw-Hill, New York, 1958.

9. J. L. Stewart, Circuit Theory and Design, Wiley and Sons, New York, 1956.

10. J. M. Miller, "Dependence of the Input Impedance of a Three-electrode Vacuum Tube Upon the Load in the Plate Circuit", National Bureau of Standards Scientific Papers, vol. 15, number 351, pp. 367-385, 1919.

11. M. E. VanValkenburg, Network Analysis, Prentice Hall, Englewood Cliffs, New Jersey, 1959.

12. J. L. Mouton, Magnetic Properties of Rare Earth-Iron Alloys, Thesis, Air Force Institute of Technology, August, 1964.

13. R. M. Bozorth, Ferromagnetism, D VanNostrand, Inc., New York, 1955.